Journal of the Mechanics and Physics of Solids 121 (2018) 409–431

Contents lists available at ScienceDirect

Journal of the Mechanics and Physics of Solids

journal homepage: www.elsevier.com/locate/jmps

Mechanics of self-healing polymer networks crosslinked by dynamic bonds

Kunhao Yu, An Xin, Qiming Wang*

Sonny Astani Department of Civil and Environmental Engineering, University of Southern California, Los Angeles, CA 90089, USA

ARTICLE INFO

Article history:
Received 21 February 2018
Revised 31 July 2018
Accepted 11 August 2018
Available online 17 August 2018

Keyword:
Self-healing
Dynamic bond
Mechanochemistry
Interpenetrating network model
Diffusion-reaction model

ABSTRACT

Dynamic polymer networks (DPNs) crosslinked by dynamic bonds have received intensive attention because of their special crack-healing capability. Diverse DPNs have been synthesized using a number of dynamic bonds, including dynamic covalent bond, hydrogen bond, ionic bond, metal-ligand coordination, hydrophobic interaction, and others. Despite the promising success in the polymer synthesis, the fundamental understanding of their self-healing mechanics is still at the very beginning. Especially, a general analytical model to understand the interfacial self-healing behaviors of DPNs has not been established. Here, we develop polymer-network based analytical theories that can mechanistically model the constitutive behaviors and interfacial self-healing behaviors of DPNs. We consider that the DPN is composed of interpenetrating networks crosslinked by dynamic bonds. The network chains follow inhomogeneous chain-length distributions and the dynamic bonds obey a force-dependent chemical kinetics. During the self-healing process, we consider the polymer chains diffuse across the interface to reform the dynamic bonds, being modeled by a diffusion-reaction theory. The theories can predict the stress-stretch behaviors of original and self-healed DPNs, as well as the healing strength in a function of healing time. We show that the theoretically predicted healing behaviors can consistently match the documented experimental results of DPNs with various dynamic bonds, including dynamic covalent bonds (diarylbibenzofuranone and olefin metathesis), hydrogen bonds, and ionic bonds. We expect our model to be a powerful tool for the self-healing community to invent, design, understand, and optimize self-healing DPNs with various dynamic bonds.

1. Introduction

Self-healing polymers have been revolutionizing the originally man-made engineering society through bringing in the autonomous intelligence that widely exists in Nature. Self-healing polymers have been applied to a wide range of engineering applications, including flexible electronics (Tee et al., 2012), energy storage (Wang et al., 2013b), biomaterials (Brochu et al., 2011), and robotics (Terryn et al., 2017). Motivated by these applications, the synthesis of self-healing polymers has received tremendous success during the past years (Binder, 2013; Roy et al., 2015; Taylor, 2016; Thakur and Kessler, 2015; van der Zwaag, 2007; Wei et al., 2014; Wojtecki et al., 2011; Wu et al., 2008; Yang and Urban, 2013). The self-healing polymers usually fall into two categories. The first category is called “extrinsic self-healing” that harnesses encapsulates of curing agents that can be released upon fractures (Blaiszik et al., 2010; Cho et al., 2006; Keller et al.,

* Corresponding author.
E-mail address: qimingw@usc.edu (Q. Wang).

https://doi.org/10.1016/j.jmps.2018.08.007
0022-5096/

Table 1
Research status of self-healing soft polymers with dynamic bonds.

Mechanism	Representative reference	Experiment	Simulation	Analytical model
Dynamic covalent bond	(Chen et al., 2002; Ghosh and Urban, 2009; Imato et al., 2012; Lu and Guan, 2012; Skene and Lehn, 2004)	Yes	No	This paper
Hydrogen bond	(Chen et al., 2012; Cordier et al., 2008; Montarnal et al., 2009; Phadke et al., 2012; Sijbesma et al., 1997; Wang et al., 2013a)	Yes	No	This paper
Ionic bond	(Das et al., 2015; Haraguchi et al., 2011; Ihsan et al., 2016; Mayumi et al., 2016; Sun et al., 2012; Sun et al., 2013; Wang et al., 2010)	Yes	No	This paper
Metal-ligand coordination	(Burnworth et al., 2011; Holten-Andersen et al., 2011; Kersey et al., 2007; Nakahata et al., 2011; Rowan and Beck, 2005; Wang et al., 2013b),	Yes	No	No
Host-guest interaction	(Liu et al., 2017a; Liu et al., 2017b)	Yes	No	No
Hydrophobic association	(Gulyuz and Okay, 2014; Okay, 2015)	Yes	No	No
π-π stacking	(Fox et al., 2012)	Yes	No	No
Nanoparticle	(Haraguchi, 2007, 2011a, b; Haraguchi et al., 2007; Haraguchi and Li, 2005; Haraguchi and Takehisa, 2002; Haraguchi et al., 2011; Huang et al., 2007; Wang et al., 2010).	Yes	(Balazs, 2007; Iyer et al., 2013)	(Wang et al., 2017)

2007; Toohey et al., 2007; White et al., 2001). These curing agents can help glue the fractured interfaces, thus restoring the mechanical property of the polymer. The second category is so-called “intrinsic self-healing” which harnesses dynamic bonds that can autonomously reform after fracture or dissociation. The dynamic bonds (Table 1) include dynamic covalent bonds (Chen et al., 2002; Ghosh and Urban, 2009; Imato et al., 2012; Lu and Guan, 2012; Skene and Lehn, 2004), hydrogen bonds (Chen et al., 2012; Cordier et al., 2008; Montarnal et al., 2009; Phadke et al., 2012; Sijbesma et al., 1997; Wang et al., 2013a), ionic bonds (Das et al., 2015; Haraguchi et al., 2011; Ihsan et al., 2016; Mayumi et al., 2016; Sun et al., 2012; Sun et al., 2013; Wang et al., 2010), metal-ligand coordinations (Burnworth et al., 2011; Holten-Andersen et al., 2011; Kersey et al., 2007; Nakahata et al., 2011; Rowan and Beck, 2005; Wang et al., 2013b), host-guest interactions (Liu et al., 2017a, b), hydrophobic interactions (Gulyuz and Okay, 2014; Okay, 2015), and π–π stacking (Fox et al., 2012).

Despite the great success in synthesis and applications of self-healing polymers, the fundamental understanding and theoretical modeling have been left behind (Table 1) (Hui and Long, 2012; Long et al., 2014; Wool, 2008; Yang and Urban, 2013). Scaling models have been proposed for the interpenetration of polymer melts (Wool and O’connor, 1981; Wool, 1995, 2008). In more recent years, molecular dynamics simulations have been employed to capture the healing properties (Balazs, 2007; Ge et al., 2014; Stukalin et al., 2013; Zhang and Rong, 2012). However, how to construct an analytical theory for modeling the physical process of the polymer networks crosslinked by various dynamic bonds is still elusive. Yu et al. (2006a) reported an analytical theory to model the interfacial welding of a polymer under relatively high temperatures; however, the welding is different from interfacial self-healing in that self-healing behaviors usually occur at relatively low temperatures. In addition, Wang et al. (2017) proposed a diffusion-governed self-healing mechanics theory to model the interfacial self-healing behaviors of nanocomposite hydrogels; however, the model is specifically designed for self-healing networks crosslinked by nanoparticles (Carlsson et al., 2010; Haraguchi, 2007, 2011a, b, 2003 ; Haraguchi and Li, 2006; Haraguchi et al., 2007; Haraguchi and Li, 2005; Haraguchi and Song, 2007; Haraguchi and Takehisa, 2002; Haraguchi et al., 2002, 2011; Huang et al., 2007; Ren et al., 2011; Wang et al., 2010). The understanding of general self-healing networks crosslinked by general dynamic bonds remains elusive. The missing of this theoretical understanding would significantly drag down the innovation of self-healing polymers to achieve their optimal self-healing performance.

Here, we consider general polymer networks crosslinked by dynamic bonds, named as dynamic polymer networks (DPNs). We model a typical healing experiment of a DPN polymer in Fig. 1. A DPN polymer with dynamic bonds in a rod sample-shape is first cut/broken into two parts, and then immediately brought into contact for a certain period of healing time. The self-healed sample is then uniaxially stretched until the sample fracture. The key process of this healing experiment is the interpenetration and bond-reformation of polymer chains with dynamic bonds around the healing interface. Here, we develop polymer-network based analytical theories that can mechanistically model the constitutive behaviors and interfacial self-healing behaviors of DPNs. We consider that the DPN is composed of interpenetrating networks crosslinked

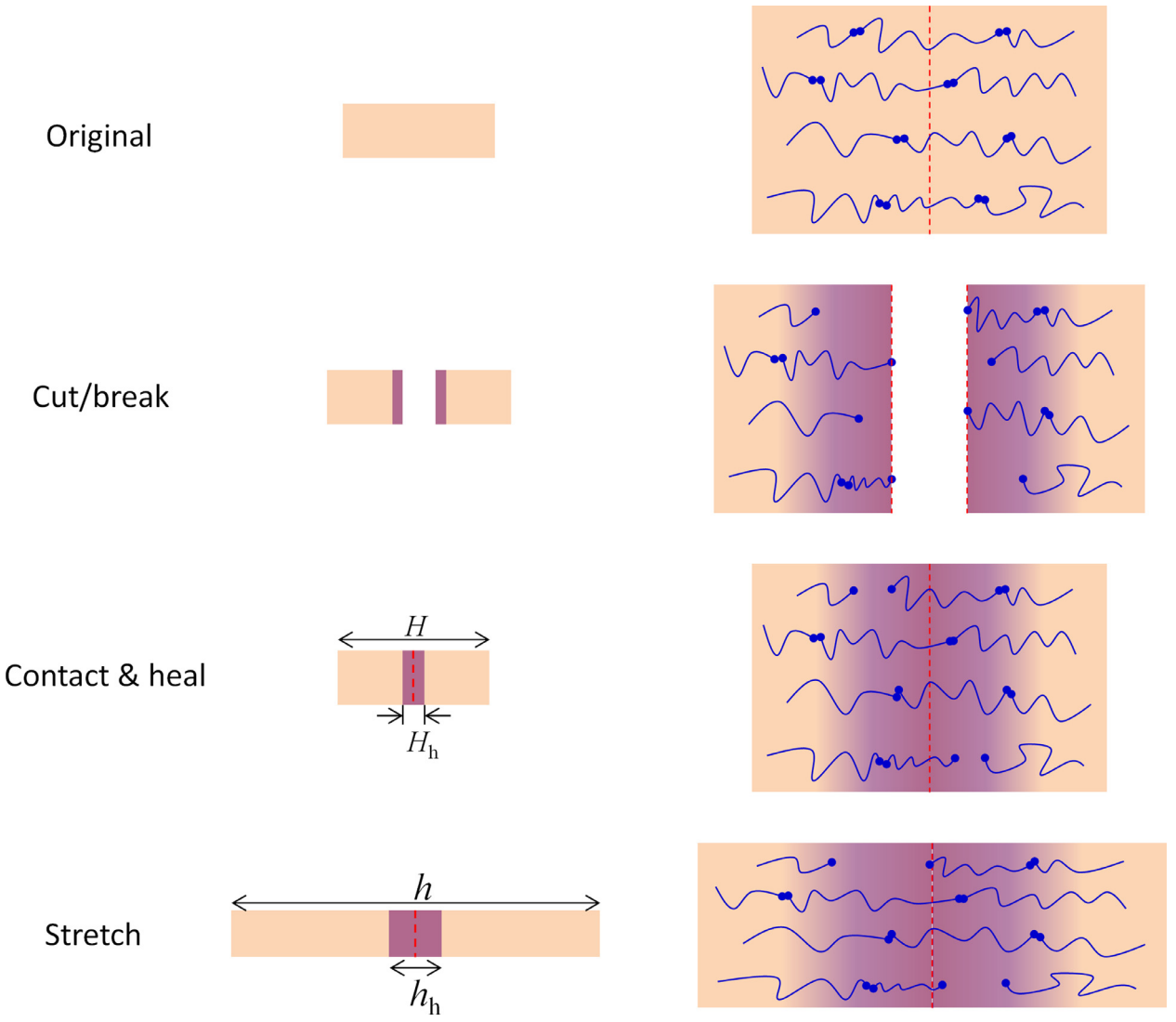

Fig. 1. Schematics to show the process of a typical self-healing experiment. An original sample is first cut/broken into two parts and then brought into contact for a healing time. Subsequently, the sample is stretched to measure the healing performance.

by dynamic bonds. The network chains follow inhomogeneous chain length-distributions and the dynamic bonds obey a force-dependent chemical kinetics. During the self-healing process, we consider the polymer chains diffuse across the interface to reform the dynamic bonds, which is modeled using a diffusion-reaction theory. The theories can predict the stress-stretch behaviors of original and self-healed DPNs. We show that the theoretically predicted healing behaviors can consistently match the documented experimental results of DPNs with various dynamic bonds, including dynamic covalent bonds (diarylbibenzofuranone and olefin metathesis), hydrogen bonds, and ionic bonds. We expect our model to become a powerful tool for the self-healing community to invent, design, understand, and optimize self-healing DPNs with various dynamic bonds.

The plan of this paper is as follows. In Section 2, we construct the theoretical frameworks for the constitutive behaviors of the original DPNs, and the interfacial self-healing behaviors of the self-healed DPNs. In Section 3, we present the theoretical results of the models and discuss the effect of chain-length distribution, bond dynamics, and chain mobility on the theoretical results. Section 4 focuses on three representative dynamic bonds including covalent dynamic bonds, hydrogen bond, and ionic bonds to discuss how the theoretical framework can be applied to explain the self-healing behaviors of these DPNs. The conclusive remarks are presented in Section 5.

2. Theoretical models

We will introduce theoretical models to first consider the constitutive behaviors of original DPNs and then the interfacial self-healing behaviors of fractured DPNs.

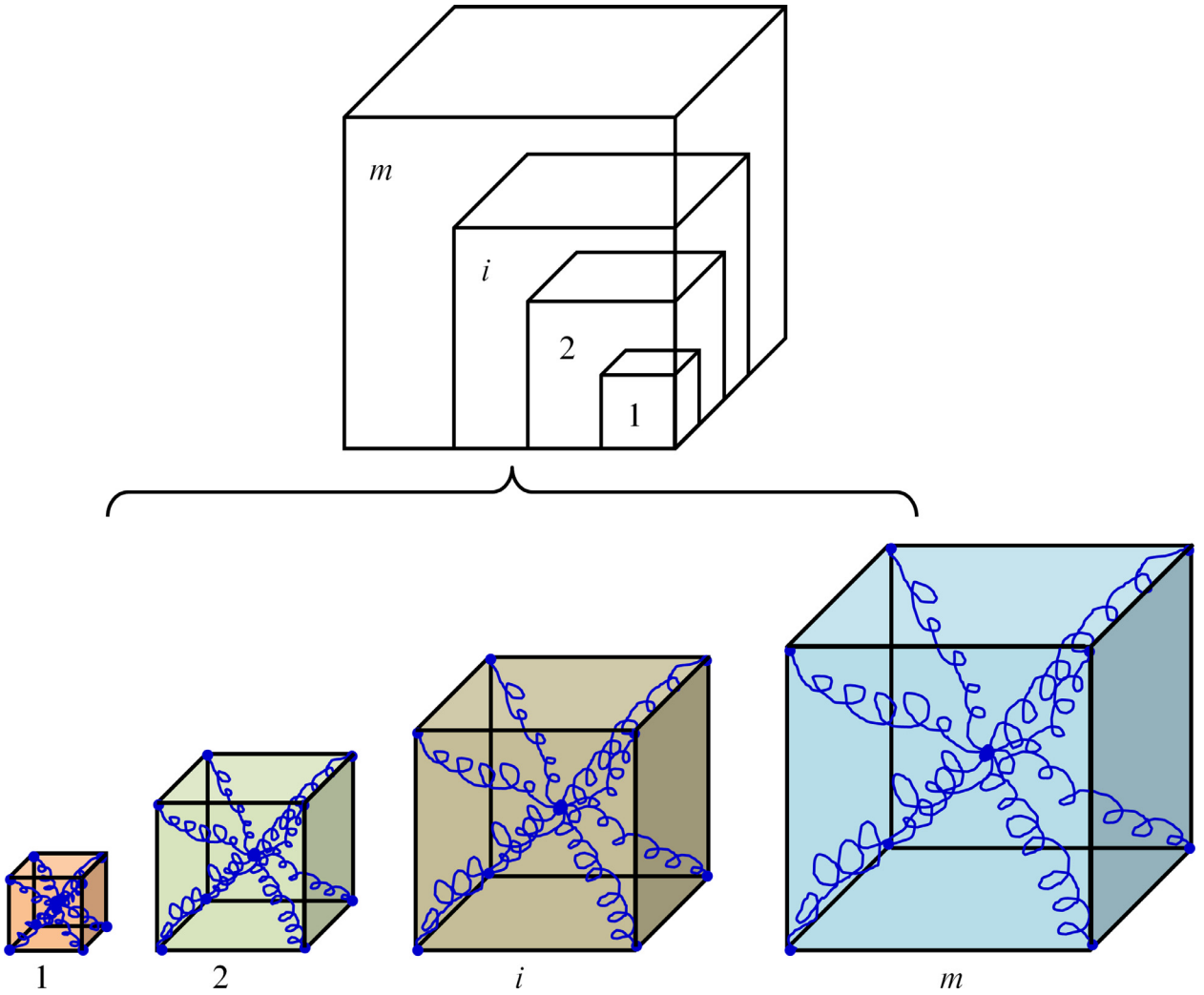

Fig. 2. Schematics to illustrate an interpenetrating network model. m types of networks interpenetrate in the material bulk space. The ith network is composed of the ith polymer chains with Kuhn segment number n_i ($1 \le i \le m$). Each type of polymer chain self-organizes into eight-chain structures.

2.1. Theory of original DPNs

2.1.1. Interpenetrating network model

We assume that the polymer is composed of m types of networks interpenetrating in the material bulk space (Fig. 2) (Wang et al., 2015). The ith network is composed of the ith polymer chains with n_i Kuhn segment number. The length of the ith chain at the freely joint state is determined by the Kuhn segment number n_i as

$$r_i^0 = \sqrt{n_i} b \tag{1}$$

where b is the Kuhn Segment length. Researchers usually denote the "chain length" as n_i (Rubinstein and Colby, 2003). Without loss of generality, the Kuhn segment number follows an order $n_1 \le n_2 \cdots \le n_m$. We denote the number of ith chain per unit volume of material as N_i. Therefore, the total chain number per unit volume of material is

$$N = \sum_{i=1}^{m} N_i \tag{2}$$

The chain number follows a statistical distribution as

$$P_i(n_i) = \frac{N_i}{N} \tag{3}$$

The summation of the statistical distribution function is a unit, i.e., $\sum_{i=1}^{m} P_i = 1$. This chain-length distribution is usually unknown if without a careful experimental examination. Although researchers usually accept that chain length is non-

uniform but should follow a chain-length distribution as shown in Eq. (3) (Erman and Mark, 1997), the most prevailing model for the rubber elasticity still considers the uniform chain length, such as three-chain model, four-chain model, and eight-chain model (Arruda and Boyce, 1993; Rubinstein and Colby, 2003; Treloar, 1975). The consideration of non-uniform chain-length to model the elasticity behaviors of rubber-like materials was recently carried out by Wang et al. (2015). Because of the limited experimental technique to characterize the chain length distribution to date, the selection of chain-length distribution is still a little ambiguous. Wang et al. (2015) tested a number of chain-length distribution functions including uniform, Weibull, normal, and log-normal, and found that the log-normal distribution can best match the material's mechanical and mechanochemical behaviors. In this paper, we will simply employ the log-normal chain-length distribution (more in Sections 3 and 4), while other distributions may also work for our model.

For the ith chain, if the end-to-end distance at the deformed state is r_i, the chain stretch is

$$\Lambda_i = \frac{r_i}{r_i^0} \tag{4}$$

The free energy of the deformed ith chain can be written as

$$w_i = n_i k_B T \left(\frac{\beta_i}{\tanh \beta_i} + \ln \frac{\beta_i}{\sinh \beta_i} \right) \tag{5}$$

where k_B is the Boltzmann constant, T is the temperature in Kelvin, $\beta_i = L^{-1}(\Lambda_i/\sqrt{n_i})$ and $L^{-1}()$ is the inverse Langevin function. Considering the chain as an entropic spring, the force within the deformed ith chain can be written as

$$f_i = \frac{\partial w_i}{\partial r_i} = \frac{k_B T}{b} \beta_i \tag{6}$$

To link the relationship between the macroscopic deformation at the material level and the microscopic deformation at the polymer chain level, we consider an interpenetrating model as shown in Fig. 2 (Wang et al., 2015). We assume the ith chains assemble themselves into regular eight-chain structures. We assume the material follows an affined deformation model (Rubinstein and Colby, 2003; Treloar, 1975), so that the eight-chain structures deform by three principal stretches (λ_1, λ_2, λ_3) under the macroscopic deformation (λ_1, λ_2, λ_3) at the material level. Therefore, the stretch of each ith chain is

$$\Lambda_i = \sqrt{\frac{\lambda_1^2 + \lambda_2^2 + \lambda_3^2}{3}} \tag{7}$$

At the undeformed state, the number of ith chain per unit material volume is N_i. However, as the material is deformed, the active ith chain is decreasing because the chain force promotes the dissociation of the dynamic bonds. We assume at the current deformed state, the number of active ith chain per unit material volume is N_i^a. Since every ith chain undergoes the same stretch Λ_i, the total free energy of the material per unit volume is

$$W = \sum_{i=1}^{m} N_i^a n_i k_B T \left(\frac{\beta_i}{\tanh \beta_i} + \ln \frac{\beta_i}{\sinh \beta_i} \right) \tag{8}$$

where $\beta_i = L^{-1}(\Lambda_i/\sqrt{n_i})$ and Λ_i is given in Eq. (7). Note that we ignore the chain entanglement effect in this interpenetration model and the following self-healing model; the entanglement contribution to hyperelastic materials can be found in other works, such as (Davidson and Goulbourne, 2013; Khiêm and Itskov, 2016; Li et al., 2016; Xiang et al., 2018).

If the material is incompressible and uniaxially stretched with three principal stretches ($\lambda_1 = \lambda$, $\lambda_2 = \lambda_3 = \lambda^{-1/2}$), the nominal stress along $\lambda_1$direction can be written as

$$s_1 = \frac{\left(\lambda - \lambda^{-2}\right) k_B T}{\sqrt{3\lambda^2 + 6\lambda^{-1}}} \sum_{i=1}^{m} \left[N_i^a \sqrt{n_i} L^{-1} \left(\sqrt{\frac{\lambda^2 + 2\lambda^{-1}}{3n_i}} \right) \right] \tag{9}$$

2.1.2. Association-dissociation kinetics of dynamic bonds

Next, we consider the association-dissociation kinetics of dynamic bonds (Fig. 3). We model the bond association and dissociation as a reversible chemical reaction (Hänggi et al., 1990; Kramers, 1940). The forward reaction rate (from associated state to dissociated state) is k_i^f and reverse reaction rate is k_i^r. For simplicity, we assume that only two ends of a chain have ending groups for the dynamic bond (Stukalin et al., 2013). If two end groups are associated, we consider this chain as "active"; otherwise, the chain is "inactive". A chemical reaction shown in Fig. 3a averagely involves one polymer chain; that is, the chemical reaction represents the transition between an active chain and an inactive chain. Here we denote the active ith chain per unit volume is N_i^a and the inactive ith chain per unit volume is N_i^d. The chemical kinetics can be written as

$$\frac{dN_i^a}{dt} = -k_i^f N_i^a + k_i^r N_i^d \tag{10}$$

Since the total number of ith chain per unit volume defined as $N_i = N_i^a + N_i^d$, the chemical kinetics can be rewritten as

$$\frac{dN_i^a}{dt} = -\left(k_i^f + k_i^r\right) N_i^a + k_i^r N_i \tag{11}$$

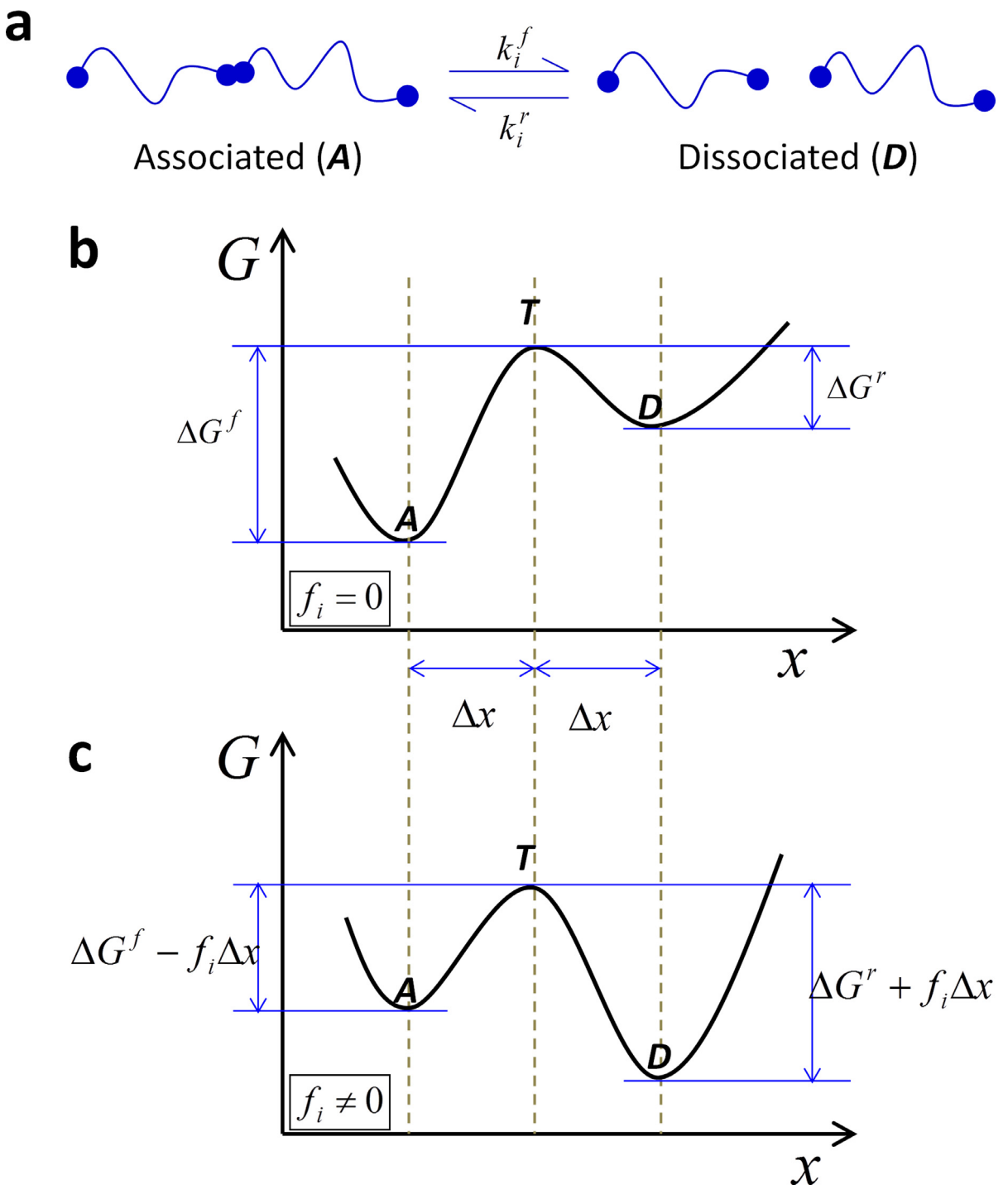

Fig. 3. (a) Schematic to show the association-dissociation kinetics of the dynamic bond on the *i*th chain. We consider the reaction from associated state to dissociated state as the forward reaction of the *i*th chain with reaction rate k_i^f $(1 \le i \le m)$, and corresponding reaction from the dissociated state to associated state as the reverse reaction with reaction rate k_i^r. (bc) Potential energy landscape of the reverse reaction of the dynamic bond on the *i*th chain with chain force (b) $f_i = 0$ and (c) $f_i \neq 0$. "A" stands for the associated state, "D" stands for the dissociated state, and "T" stands for the transition state.

At the as-fabricated undeformed state, the reaction rates are $k_i^f = k_i^{f0}$ and $k_i^r = k_i^{r0}$, respectively. As the material is fabricated as an integrated solid, we simply assume the association reaction is much stronger than the dissociation reaction at the fabricated state, i.e., $k_i^{f0} << k_i^{r0}$. Therefore, most of the ith chains are at the associated state, as the equilibrium value of N_i^a at the undeformed state is

$$N_i^a = \frac{k_i^{r0}}{k_i^{r0} + k_i^{f0}} N_i \approx N_i \tag{12}$$

At the deformed state, the ith chain is deformed with stretch Λ_i. Since the bond strength of the dynamic bonds is much weaker than those of the permanent bonds such as covalent bonds, the chain force would significantly alter the bonding reaction (Hänggi et al., 1990; Kramers, 1940). Specifically, the chain force tends to pull the bond open to the dissociated state. This point has been well characterized by Bell model for the ligand-receptor bonding for the cell adhesion behaviors, as well as for biopolymers (Bell, 1978). We here adopt the Bell-like model and consider the energy landscape between the associated state and dissociated state as shown in Fig. 3b (Wang et al., 2015). We consider an energy barrier exists between the associated state (denoted as "A") and dissociated state ("D") through a transition state ("T"). At the undeformed state of the ith chain, the energy barrier for A→D transition is ΔG^f and the energy barrier for D→Atransition is ΔG^r. Under the deformed state of the ith chain, the chain force f_i lowers down the energy barrier of A→D transition to $\Delta G^f - f_i \Delta x$ and increases the energy barrier for D→A transition to $\Delta G^r + f_i \Delta x$, where Δx is the distance along the energy landscape coordinate (Fig. 3c). Since the occurrence of the chemical reaction requires the overcoming of the energy barriers, the higher energy barrier is corresponding to the lower likelihood of the reaction. According to the Bell model, the reaction rates are governed by the energy barrier through exponential functions as (Bell, 1978; Ribas-Arino and Marx, 2012).

$$k_i^f = A \exp\left(-\frac{\Delta G^f - f_i \Delta x}{k_B T}\right) = k_i^{f0} \exp\left(\frac{f_i \Delta x}{k_B T}\right) \tag{13a}$$

$$k_i^r = B \exp\left(-\frac{\Delta G^r + f_i \Delta x}{k_B T}\right) = k_i^{r0} \exp\left(-\frac{f_i \Delta x}{k_B T}\right) \tag{13b}$$

Where A and B are constants and Δx is treated as a fitting parameter for a given material.

We first consider the initially-undeformed material is suddenly loaded with a deformation state ($\lambda_1 = \lambda,\ \lambda_2 = \lambda_3 = \lambda^{-1/2}$) at $t = 0$ and then deformation remains constant. The reaction rates are time-independent. Therefore, the active ith chain number per unit material volume can be calculated as

$$N_i^a = \exp\left[-\int_0^t \left(k_i^{f0} \exp\left(\frac{f_i \Delta x}{k_B T}\right) + k_i^{r0} \exp\left(-\frac{f_i \Delta x}{k_B T}\right)\right) d\tau\right] \left[\int_0^t \frac{k_i^{r0} \exp\left(-\frac{f_i \Delta x}{k_B T}\right) N_i}{\exp\left[-\int_0^\tau \left(k_i^{f0} \exp\left(\frac{f_i \Delta x}{k_B T}\right) + k_i^{r0} \exp\left(-\frac{f_i \Delta x}{k_B T}\right)\right) d\varsigma\right]} d\tau + N_i\right] \tag{14}$$

In Eq. (14), the force f_i in the ith chain is constant. Therefore, we can rewrite Eq. (14) as

$$\frac{N_i^a}{N_i} = \frac{k_i^{r0} \exp\left(-\frac{f_i \Delta x}{k_B T}\right) + k_i^{f0} \exp\left(\frac{f_i \Delta x}{k_B T}\right) \exp\left[-\left(k_i^{f0} \exp\left(\frac{f_i \Delta x}{k_B T}\right) + k_i^{r0} \exp\left(-\frac{f_i \Delta x}{k_B T}\right)\right) t\right]}{k_i^{f0} \exp\left(\frac{f_i \Delta x}{k_B T}\right) + k_i^{r0} \exp\left(-\frac{f_i \Delta x}{k_B T}\right)} \tag{15}$$

Over a period of loading time, the active ith chain number per unit volume N_i^a in Eq. (15) decreases from N_i to a plateau with a value $N_i k_i^{r0} \exp\left(-\frac{f_i \Delta x}{k_B T}\right) / \left[k_i^{f0} \exp\left(\frac{f_i \Delta x}{k_B T}\right) + k_i^{r0} \exp\left(-\frac{f_i \Delta x}{k_B T}\right)\right]$ (Fig. 4a). The required timescale is the characteristic time scale of the chemical reaction.

If the material is loaded with increasing stretch ($\lambda_1 = \lambda,\ \lambda_2 = \lambda_3 = \lambda^{-1/2}$), the chemical reaction rates are both time-dependent. In solving the chemical kinetics, we have to consider the time-dependent behavior of the reaction rates and solve the equation numerically. In a more common case, we apply the load with a very small loading rate, so that the deformation of the material is usually assumed as quasi-static. It means that in every small increment of the load, the chemical reaction already reaches its equilibrium state with an equilibrium active ith chain numberN_i^a. Under this condition, the active ith chain number per unit material volume is expressed as

$$N_i^a = \frac{N_i k_i^{r0} \exp\left(-\frac{f_i \Delta x}{k_B T}\right)}{k_i^{f0} \exp\left(\frac{f_i \Delta x}{k_B T}\right) + k_i^{r0} \exp\left(-\frac{f_i \Delta x}{k_B T}\right)} \tag{16}$$

with the chain force f_i as expressed in Eq. (6). As shown in Fig. 4b, N_i^a decreases from N_i to near-zero at various speeds for various chain lengths, because different chain lengths are corresponding to different chain forces. Once N_i^a is solved, it can be plugged into Eq. (9) to obtain the stress-stretch behaviors of the DPNs. As shown from Eq. (16), the density of active ith chain should decrease as the chain force increases. This molecular picture is different from the dynamic polymers with bond exchange reactions, for which the density of associated bonds is assumed as constant during the network evolution (Yu et al., 2016a).

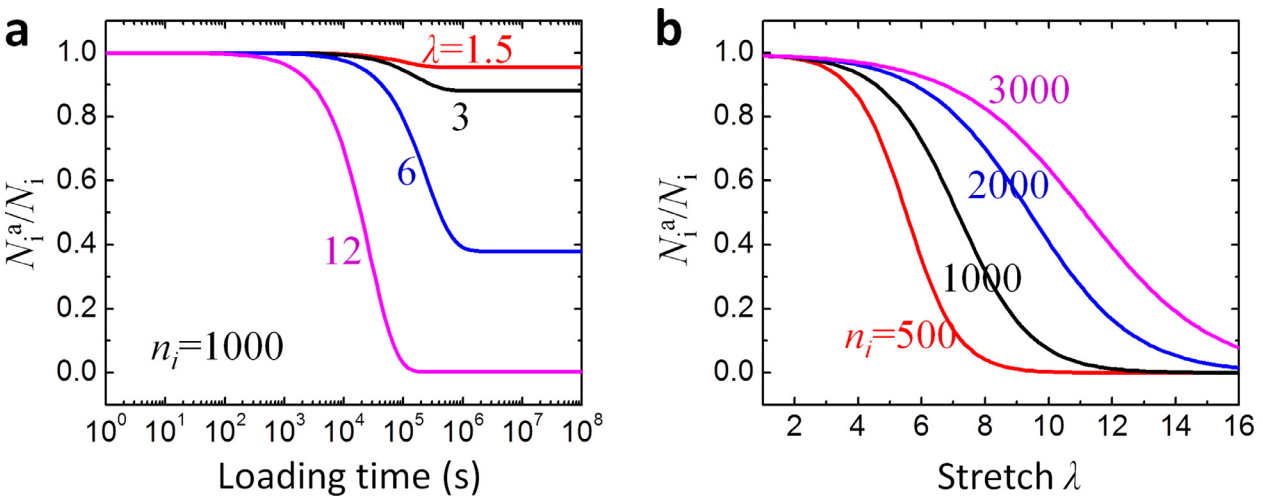

Fig. 4. Examples of chain dynamics behaviors. (a) The active *i*th chain number in functions of the loading time of various constant uniaxial stretch. (b) The active *i*th chain number of various chain length n_i in functions of the quasi-statically increasing uniaxial stretch. The used parameters can be found in Table 2.

2.1.3. Additional consideration

In addition to the above association-dissociation kinetics, we also consider two supplementary points. The first one is the network alteration. During the mechanical loading, a portion of dissociated short chains may reorganize to become active long chains (Chagnon et al., 2006; Marckmann et al., 2002). To capture this effect, we follow the network alteration theory to model the number of active chains to be an exponential function of the chain stretch Λ_i as

$$\frac{N_i^a}{N_i} = \exp\left[\alpha(\Lambda_i - 1)\right] \tag{17}$$

where α is the chain alteration parameter. Similar network alteration model has been employed to model the chain reorganization for the Mullin's effect of rubber (Chagnon et al., 2006; Marckmann et al., 2002), double-network hydrogels (Zhao, 2012), and nanocomposite hydrogels (Wang and Gao, 2016). It has been shown that the network alteration is a unique network damage mechanism that facilitates the stiffening effect of the stress-stretch curve (Chagnon et al., 2006; Marckmann et al., 2002; Wang and Gao, 2016). Since the effect of network alteration on the stress-strain behaviors of polymer networks has been clearly demonstrated in the existing literature (Wang and Gao, 2016), we would not discuss in details about their effects in this paper, and just harness this network alteration effect to better capture the stress-stretch curve shapes of the original DPNs.

The second point is about the full dissociation when the chain length is longer than the length limit of the chain. The fully extended length of the *i*th chain is $n_i b$with a stretch as $n_i b/(\sqrt{n_i} b) = \sqrt{n_i}$. If the stretch of the *i*th chain is larger than $\sqrt{n_i}$, the dynamic bond will be fully dissociated. This can be expressed as

$$N_i^a = 0, \text{ if } \Lambda_i \geq \sqrt{n_i} \tag{18}$$

2.2. Self-healing behavior of fractured DPNs

We consider a DPN polymer sample shown in Fig. 1. We cut the sample into two parts and then immediately contact back. After a certain period of healing time *t*, the sample is uniaxially stretched until breaking into two parts again. If the healing is not fully, the breaking point will be at the healing interface; however, if the healing is close to 100%, the breaking point should be distributed stochastically through the whole sample. Here, we consider the self-healed sample is composed of two segments (Fig. 1). Around the healing interface, the polymer chain would diffuse across the interface to form new networks through forming new dynamic bonds. We call this region as "self-healed segment". Away from the self-healed segment, the polymer networks are intact, and we call this region as "virgin segment".

2.2.1. Behavior of the self-healed segment

As we assume in Section 2.1.1, the *i*th chains form network following eight-chain structures (Fig. 5a). For simplicity of analysis, we assume the cutting position is located at a quarter part of the eight chain cube, namely the center position between a corner and the center of the eight-chain cube (Fig. 5a). The cutting process forces the polymer chains to be dissociated from the dynamic bond around the corner or center positions. This assumption is based on the Lake-Thomas theory that assumes that the chain force is transferred through every Kuhn segment on the chain, and under the same chain force, the dynamic bonds with much weaker strengths are expected to break sooner than the permanent bonds (Lake and

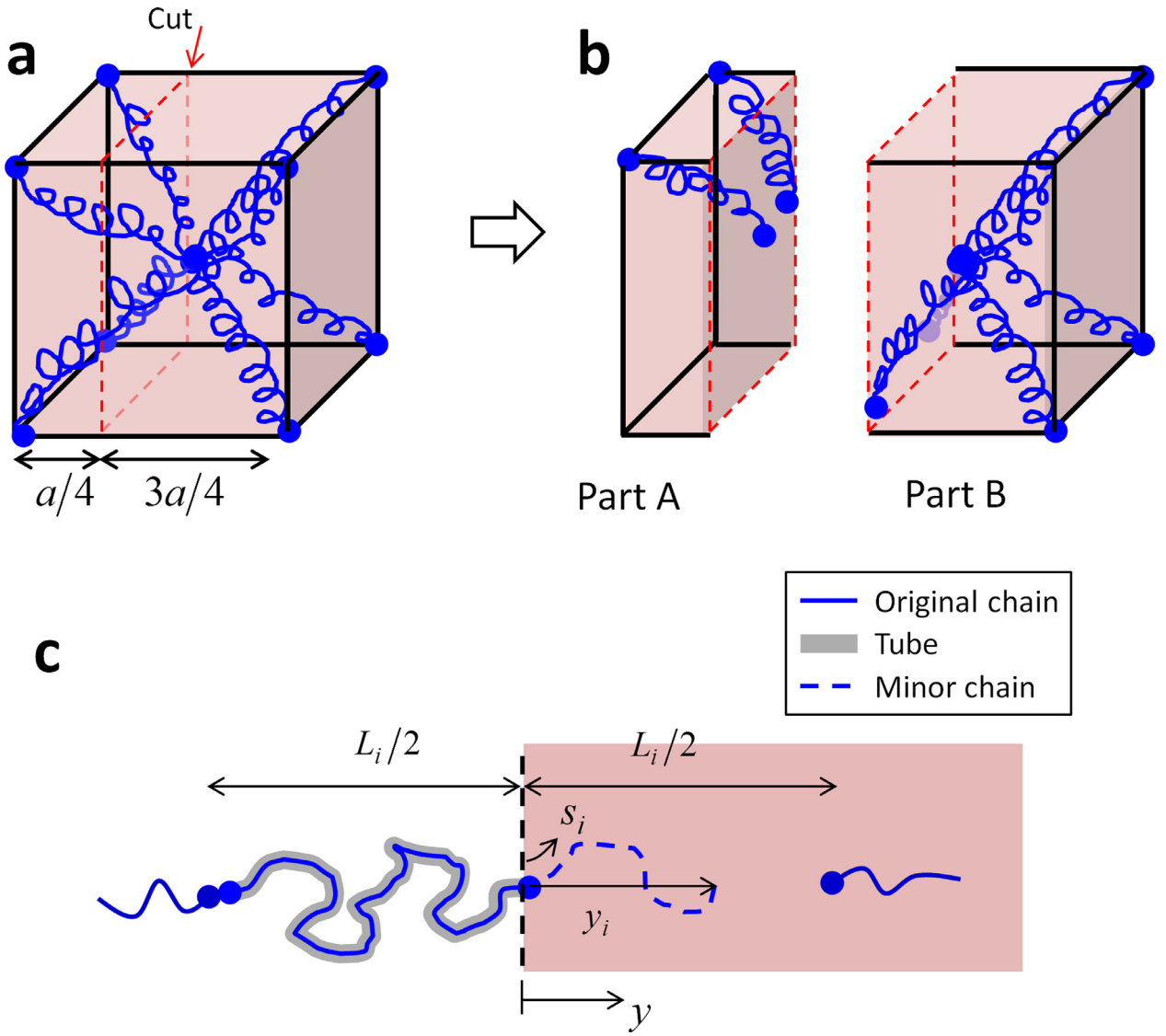

Fig. 5. (a, b) Schematics of the eight-chain network model before and after the cutting process. The cutting is assumed to be located in a quarter position of the cube. (c) A schematic to show the diffusion behavior of the *i*th polymer chain across the interface.

Thomas, 1967). Since we immediately contact the material back, we assume the ending groups of the dynamic bonds are still located around the cutting interface, yet without enough time to migrate into the material matrix (Fig. 5b) (Wang et al., 2017). Driven by weak interactions between ending groups of the dynamic bonds, the ending groups on the interface will diffuse across the interface to penetrate into the matrix of the other part of the material to form new dynamic bonds. Specifically in Fig. 5b, the ending groups of the part A will penetrate into part B towards the center position of the cube, and the ending groups of part B will penetrate into Part A towards the corner positions of the cube. These interpenetration behaviors can be simplified as a 1D model shown in Fig. 5c. As shown in Fig. 5c, an open ending group around the interface penetrates into the other part of the material to find another open ending group to form a dynamic bond. Once the dynamic bond reforms, the initially “inactive” chain becomes “active”. This behavior can be understood as two processes: chain diffusion and ending group reaction.

To model the chain diffusion, we consider a reptation-like model shown in Fig. 5c (De Gennes, 1979; de Gennes, 1971; Doi and Edwards, 1978; Rubinstein and Colby, 2003). We assume the polymer chain diffuses along its contour tube analogous to the motion of a snake. The tube diameter is assumed as much smaller than the chain length. The motion of the polymer chain is enabled by extending out small segments called “minor chains”. The curvilinear motion of the polymer chain is

characterized by the Rouse friction model with the curvilinear diffusion coefficient of the ith chain written as

$$D_i = \frac{k_B T}{n_i \xi} \tag{19}$$

where ξ is the Rose friction coefficient per unit Kuhn segment. In the original reptation model, the contour length of the primitive chain is considered as $n_i b^2/a$, where a is a step length of the primitive chain (de Gennes, 1971; Doi and Edwards, 1988). The step length a is an unknown parameter that depends on the statistical nature of the network and is of the order of the mesh side of the network. Conceptually, we may assume $a = b$, then the contour length of the primitive chain will be approximated as $n_i b$.

We note that the chain motion follows a curvilinear path; therefore, we construct two coordinate systems s and y, where s denotes the curvilinear path along the minor chains and y denotes the linear path from the interface to the other open ending group. When the ith chain moves $s_i$distance along the curvilinear path, it is corresponding to $y_i$distance along y coordinate. Here we assume the selection of the curvilinear path is fully stochastic following the Gaussian statistics (Kim and Wool, 1983; Whitlow and Wool, 1991; Zhang and Wool, 1989). Therefore, the conversion of the distances in two coordinate systems is expressed as

$$y_i = \sqrt{s_i b} \tag{20}$$

According to the eight-chain cube assumption, the distance between the corner and the center within the ith network cube at its freely joint state is

$$L_i \approx \sqrt{n_i} b \tag{21}$$

The distance between the ending group around the interface and the other ending group in the matrix is $L_i/2$. According to Eq. (21), the positions $y = 0$ and $y = L_i/2$ are corresponding to $s = 0$ and $s = L_i^2/4b$, respectively.

If we only consider the polymer chain diffusion, the diffusion of the ith chain can be modeled with the following diffusion equation along the curvilinear coordinate s,

$$\frac{\partial C_i^d(t,s)}{\partial t} = D_i \frac{\partial^2 C_i^d(t,s)}{\partial s^2} \tag{22}$$

where $C_i^d(t,s)$ is the inactive ith chain number per unit length (with unit area) along the coordinate s ($0 \le s \le L_i^2/4b$) at time t. However, the chain behavior is more complicated than just diffusion, because during the diffusion the ending group would encounter another ending group to undergo a chemical reaction to form a new dynamic bond. Although the chemical reaction may only occur around the ending group within the material matrix (relatively immobile ending group at$s = L_i^2/4b$), the reaction forms dynamic bonds to transit an inactive chain into an active chain, and this reaction would reduce the amount of the inactive ending groups and further drive the motion of the other inactive ending groups. Therefore, the chain diffusion and ending group reaction actually are strongly coupled. Therefore, we consider an effective diffusion-reaction model to consider the effective behaviors of the chain and the ending group as (Crank, 1979)

$$\frac{\partial C_i^d(t,s)}{\partial t} = D_i \frac{\partial^2 C_i^d(t,s)}{\partial s^2} - \frac{\partial C_i^a(t,s)}{\partial t} \tag{23}$$

$$\frac{\partial C_i^a(t,s)}{\partial t} = k_i^{r0} C_i^d(t,s) - k_i^{f0} C_i^a(t,s) \tag{24}$$

where $C_i^a(t,s)$ is the active ith chain number per unit length (with unit area) along the coordinate s ($0 \le s \le L_i^2/4b$) at time t. As the polymer chain is freely joint during the diffusion process, we here use the chemical reaction rates k_i^{f0} and k_i^{r0}.

In the initial state of the self-healing, all mobile open-ending groups of the ith chains are located around the healing interface. Therefore, the initial condition of the diffusion-reaction model is

$$C_i^d(t=0,s) = N_i \delta(s) \tag{25}$$

$$C_i^a(t=0,s) = 0 \tag{26}$$

where $\int_{-\infty}^{\infty} \delta(s) ds = 1$.

For a self-healing polymer that is capable of forming a stable solid form and enabling relatively short healing time, the basic requirement is $k_i^{f0} < k_i^{r0}$. This requirement means that the association reaction is stronger than the dissociate reaction. Otherwise, the polymer is unstable under external perturbations. Here, we further focus our attention on polymers with good healing capability, so that the polymers can easily self-heal under relatively mild conditions. This requirement further implies that k_i^{r0} should be much larger thank_i^{f0}, i.e., $k_i^{r0} >> k_i^{f0}$. Under this condition, Eqs. (23) and (24) can be reduced as

$$\frac{\partial C_i^d(t,s)}{\partial t} = D_i \frac{\partial^2 C_i^d(t,s)}{\partial s^2} - k_i^{r0} C_i^d(t,s) \tag{27}$$

At the same time, around the locations $= L_i^2/4b$, all open ending groups form dynamic bonds. This leads to the vanishing of inactive chains around the location $s = L_i^2/4b$, written as

$$C_i^d\left(t, s = L_i^2/4b\right) = 0 \tag{28}$$

Along with above initial and boundary conditions, the reaction-diffusion equation (Eq. (27)) can be solved analytically or numerically.

Once $C_i^d(t,s)$ in the diffusion-reaction model (Eq. (27)) is solved, we can further obtain the active ith chain number per unit volume of the self-healing segment at healing time t, written as

$$\frac{N_i^h(t)}{N_i} = 1 - \frac{4b}{L_i^2}\int_0^{L_i^2/4b} \frac{C_i^d(t,s)}{N_i} ds \tag{29}$$

where $N_i^h(t)$ is for the self-healed segment at the undeformed state ($\lambda_1 = \lambda_2 = \lambda_3 = 1$), and the superscript "$h$" denotes "healed".

At the deformed state, the active ith chain number in the self-healed segment decreases with the increasing stretch. If we consider a quasistatic load with principal stretches ($\lambda_1 = \lambda^h,\ \lambda_2 = \lambda_3 = (\lambda^h)^{-1/2}$), the active ith chain number per unit volume of the self-healing segment can be calculated as

$$N_i^{ah}(t) = \frac{N_i^h(t) k_i^{r0} \exp\left(-\frac{f_i \Delta x}{k_B T}\right)}{k_i^{f0} \exp\left(\frac{f_i \Delta x}{k_B T}\right) + k_i^{r0} \exp\left(-\frac{f_i \Delta x}{k_B T}\right)} \tag{30}$$

with the chain force expressed as

$$f_i = \frac{k_B T}{b} L^{-1}\left(\sqrt{\frac{\left(\lambda^h\right)^2 + 2\left(\lambda^h\right)^{-1}}{3n_i}}\right) \tag{31}$$

Therefore, the free energy per unit volume of the self-healed segment can be written as

$$W^h = \sum_{i=1}^{m} N_i^{ah}(t) n_i k_B T\left(\frac{\beta_i^h}{\tanh \beta_i^h} + \ln \frac{\beta_i^h}{\sinh \beta_i^h}\right) \tag{32}$$

where $\beta_i^h = L^{-1}(\sqrt{[(\lambda^h)^2 + 2(\lambda^h)^{-1}]/3n_i})$ and $N_i^{ah}(t)$ is given by Eq. (30). The nominal stress along λ_1 direction can be written as

$$s_1^h\left(\lambda^h, t\right) = \frac{\left(\lambda^h - \lambda^{h-2}\right) k_B T}{\sqrt{3\left(\lambda^h\right)^2 + 6\left(\lambda^h\right)^{-1}}} \sum_{i=1}^{m}\left[N_i^{ah}(t)\sqrt{n_i} L^{-1}\left(\sqrt{\frac{\left(\lambda^h\right)^2 + 2\left(\lambda^h\right)^{-1}}{3n_i}}\right)\right] \tag{33}$$

where t is the healing time and λ^h is the uniaxial stretch in the self-healed segment.

2.2.2. Behavior of the self-healed sample

We consider a self-healed sample (length H) with a self-healed segment (length H^h, $H^h << H$) and two virgin segments (Fig. 1). Under a uniaxial stretch, the lengths of the whole sample and the self-healed segment become h and h^h, respectively. The stretch of the self-healed segment is $\lambda^h = h^h/H^h$. The stretch of the virgin segment is approximately equal to the stretch of the whole sample λ because $\lambda = h/H \approx (h - h^h)/(H - H^h)$. We assume the initial cross-sections of the virgin segment and the self-healed segment are the same; then, the uniaxial nominal stresses in the self-healed segment and the virgin segment should be equal, written as

$$s_1^h\left(\lambda^h\right) = s_1(\lambda) \tag{34}$$

where $s_1^h(\lambda^h)$ is referred to Eq. (33), and $s_1(\lambda)$is referred to Eq. (9). From Eq. (34), we can determine the stress-stretch behaviors of the self-healed sample for various healing time t.

3. Results of the theoretical models

We first discuss results of the diffusion-reaction model for the interpenetration of polymer chains, and then predict the stress-stretch behaviors of original DPNs and self-healing DPNs. We further predict the healing strength in a function of the healing time, and discuss how chain distribution, chain mobility, and bond reaction dynamics affect the healing behavior.

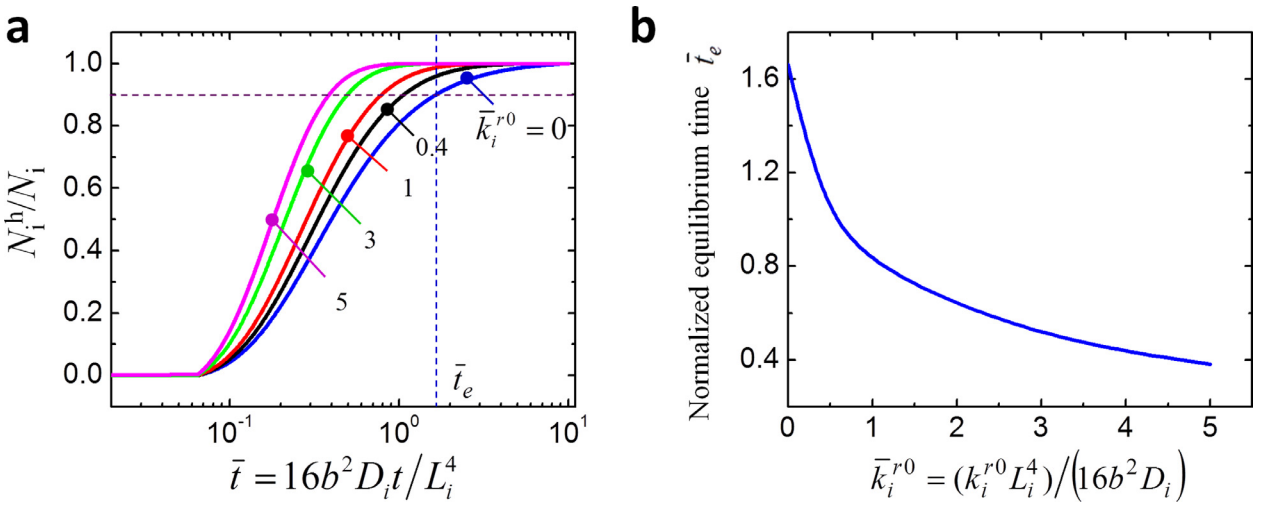

Fig. 6. (a) The normalized healed ith chain number in functions of normalized time $\bar{t}=16b^2D_it/L_i^4$ for various normalized reverse reaction rate $\bar{k}_i^{r0}=(k_i^{r0}L_i^4)/(16b^2D_it)$. (b) The normalized equilibrium time $\bar{t}_e$ in a function of the normalized reverse reaction rate.

3.1. Diffusion-reaction around the interface

Using the Danckwert's method, we can solve $C_i^d(t,s)$ in Eq. (27) as (Crank, 1979)

$$C_i^d(t,s)=k_i^{r0}\int_0^t \bar{C}_i^d(\tau,s)\exp(-k_i^{r0}\tau)d\tau+\bar{C}_i^d(t,s)\exp(-k_i^{r0}t) \tag{35}$$

$$\bar{C}_i^d(t,s)=\frac{2N_i}{\sqrt{4\pi D_it}}\left[\exp\left(-\frac{s^2}{4D_it}\right)-\exp\left(-\frac{\left(s-L_i^2/2b\right)^2}{4D_it}\right)\right] \tag{36}$$

Through Eq. (29), we can obtain the healed ith chain number $N_i^h(t)$ in a function of the healing time t. As shown in Fig. 6a, we plot the normalized healed ith chain number $N_i^h(t)/N_i$ in functions of normalized healing time $\bar{t}=16b^2D_it/L_i^4$ for various normalized reverse reaction rate $\bar{k}_i^{r0}=(k_i^{r0}L_i^4)/(16b^2D_it)$. The initially zero normalized healed ith chain number gradually increases until the plateau 1. Here, we define the time for 90% healing as the equilibrium diffusion-reaction time t_e. We find that t_e decreases as increasing reverse reaction rate (Fig. 6b). It is because higher reverse reaction rate would drive the movement of the polymer chain to be faster, thus enabling a smaller t_e.

3.2. Stress-strain behaviors of original and self-healed DPNs

In this section, we discuss examples of stress-stretch behaviors of original and self-healed DPNs. For simplicity, we only consider a log-normal chain length distribution as (Wang et al., 2015)

$$P_i(n_i)=\frac{1}{n_i\delta\sqrt{2\pi}}\exp\left[-\frac{(\ln n_i-\ln n_a)^2}{2\delta^2}\right] \tag{37}$$

where $n_a$and δ are the mean of $n_i$and standard deviation of $\ln n_i$, respectively. As an example, we plot a chain length distribution shown in Fig. 7a. As discussed in Section 2.1.2, the application of the stretching force would destabilize the association-dissociation kinetics of the dynamic bonds and decrease the number of active chains. As the stretch increases, the corresponding stress first increases. As the decreased active chain number reaches a certain level, the stress reaches a peak point and then begins to decrease (Fig. 7b). Stress at the peak point is corresponding to the strength of the DPN $s_{\max}$.

As the self-healed sample, we first calculate the healed ith chain number $N_i^h(t)$ in the self-healed segment, and then obtain the self-healed stress-strain behaviors from Eq. (33). Using Eq. (34), we subsequently determine the stress-stretch behavior of the self-healed sample that is composed of a self-healed segment and two virgin segments (Fig. 7c). We plot the example stress-stretch behaviors of the self-healed samples for various healing time in Fig. 7c. We define a parameter called healing strength ratio $\eta=s_{\max}^h/s_{\max}$, where $s_{\max}^h$is the strength of the self-healed sample under uniaxial stretch. The healing strength ratio η increases with increasing healing time t until the plateau 100% (Fig. 7d). We further define the healing time corresponding to 90% healing strength ratio as the equilibrium healing time t_{eq}.

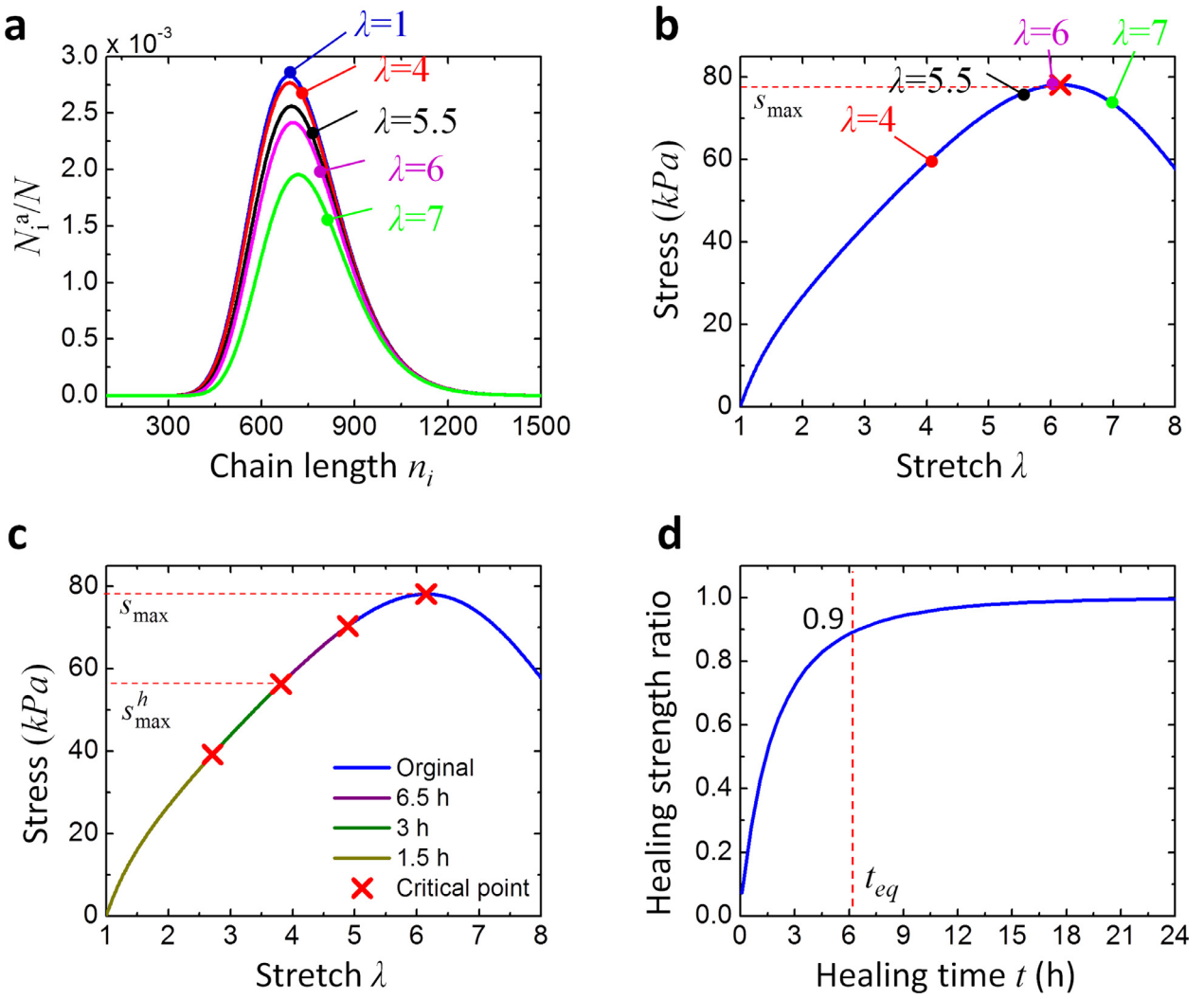

Fig. 7. (a) Active *i*th chain number distribution evolution under various uniaxial stretches. (b) The predicted stress-stretch behaviors of the original sample under quasi-statically increasing uniaxial stretches. (c) Predicted stress-stretch curves of original and self-healed samples under quasi-statically increasing uniaxial stretches. (d) The predicted healing strength ratio in a function of healing time. The healing time corresponding to 90% healing strength ratio is defined as the equilibrium healing time t_{eq}. The used parameters can be found in Table 2.

3.3. Effect of key parameters on healing behaviors

Once the calculation methods for the stress-stretch behaviors of the original and self-healed DPNs are established, we further discuss the effects of some key factors on the healing behaviors in this section. These factors include the chain length, the chain mobility, and the bond dynamics.

3.3.1. Effect of chain length

We consider the chain length within the polymer matrix follows a certain log-normal distribution. The probability of the chain length distributes over a wide range with the highest probability at the average chain length n_a. As the average chain length n_a changes, the chain length distribution shifts (Fig. 8a). With increasing average chain length n_a, the original DPN becomes more stretchable (Fig. 8b). At the same time, according to Eq. (19), the effective diffusion coefficient decreases as the average chain length increases. With the same bond kinetics, the healing process of the DPN should become slower. As shown in Fig. 8c and d, the theory predicts that the equilibrium healing time of the DPN increases with increasing average chain length n_a.

3.3.2. Effect of chain mobility

The chain mobility is represented by the Rouse friction coefficientξ. When the chain is less mobile within the matrix, the Rouse friction coefficient ξ becomes larger. Rouse friction coefficient ξ may not affect the stress-stretch behaviors of

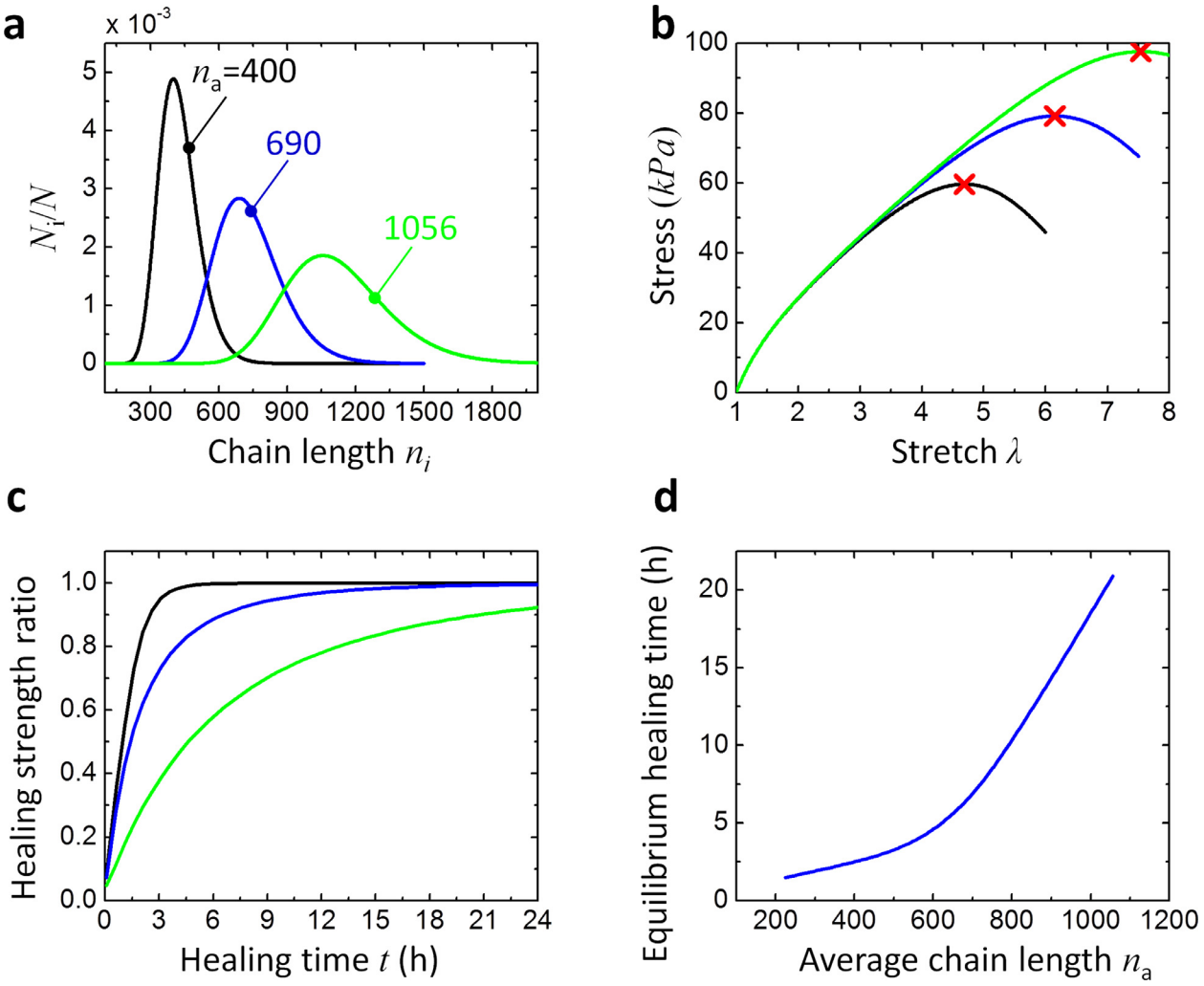

Fig. 8. Effect of chain length distribution on the healing behaviors. (a) The chain length distributions for various average chain length n_a. (b) The predicted stress-stretch curves of the original sample under quasi-statically increasing uniaxial stretches. (c) The predicted healing strength ratios in functions of healing time. (d) The predicted equilibrium healing time t_{eq} in a function of average chain length n_a. The used parameters are the same as those used in Fig. 7 except n_a.

the original DPNs. However, according to Eq. (19), the effective diffusion coefficient of the polymer chains decreases as the Rouse friction coefficient ξ increases, and subsequently, the healing process becomes slower. As shown in Fig. 9a and b, the equilibrium healing time of the DPN increases with increasing Rouse friction coefficient ξ.

3.3.3. Effect of bond dynamics

The association-dissociation bond dynamics is represented by the forward and reverse reaction rates of the ith chain $k_i^{f0}$and k_i^{r0}, respectively. As we consider the forward reaction rate is much smaller than the reverse reaction rate, we fix forward reaction rate as $k_i^{f0} = 2 \times 10^{-7} s^{-1}$and vary the reverse reaction rate k_i^{r0} to examine its effect on the healing behavior (Fig. 10). With increasing reverse reaction rate k_i^{r0} (reverse reaction is from dissociated state to the associated state), the associated state is less likely to be destabilized by the chain force; therefore, the strength and stretchability of the original DPNs increase (Fig. 10a). During the self-healing process, the higher reverse reaction rate promotes the re-formation of the dynamic bonds, thus speeding the healing process. Therefore, with increasing reverse reaction rate k_i^{r0}, the equilibrium healing time of the DPNs decreases (Fig. 10b and c).

It is noted that during the self-healing process, two processes coexist: chain diffusion and association-dissociation bond dynamics. As k_i^{r0}increases to a sufficiently large value, the bond dynamics timescale is much smaller than the chain diffusion timescale. Under this condition, the self-healing timescale is mainly governed by the chain diffusion, and the change of the reverse reaction rate may not affect the self-healing time scale anymore. As shown in Fig. 10c, when $k_i^{r0} > 3 \times 10^{-4} s^{-1}$, the equilibrium healing time only changes slightly with increasing reverse reaction rate k_i^{r0}.

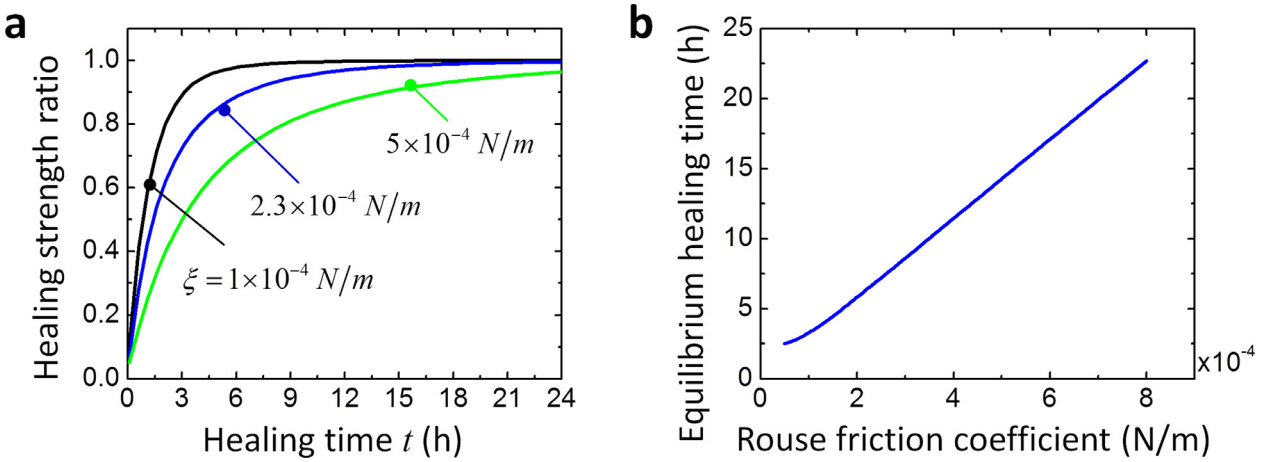

Fig. 9. Effect of chain mobility on the healing behaviors. (a) The predicted healing strength ratios in functions of healing time for various Rouse friction coefficients ξ. (b) The predicted equilibrium healing time t_{eq} in a function of Rouse friction coefficients. The used parameters are the same as those used in Fig. 7 except Rouse friction coefficients ξ.

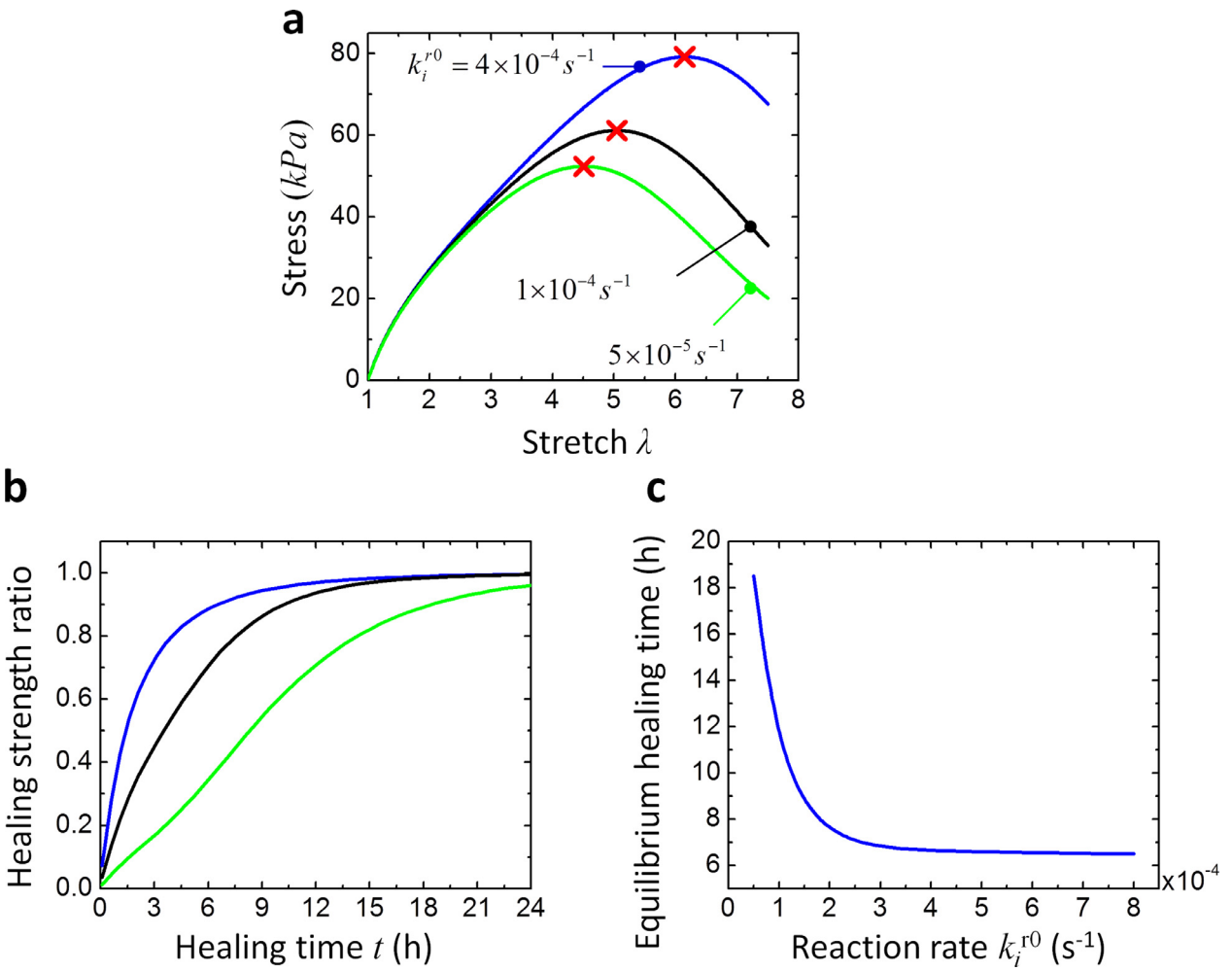

Fig. 10. Effect of bond dynamics on the healing behaviors. (a) The predicted stress-stretch curves of the original sample under quasi-statically increasing uniaxial stretches. (b) The predicted healing strength ratios in functions of healing time. (c) The predicted equilibrium healing time t_{eq} in a function of reverse reaction rates k_i^{r0}. The used parameters are the same as those used in Fig. 7 except reverse reaction rates k_i^{r0}.

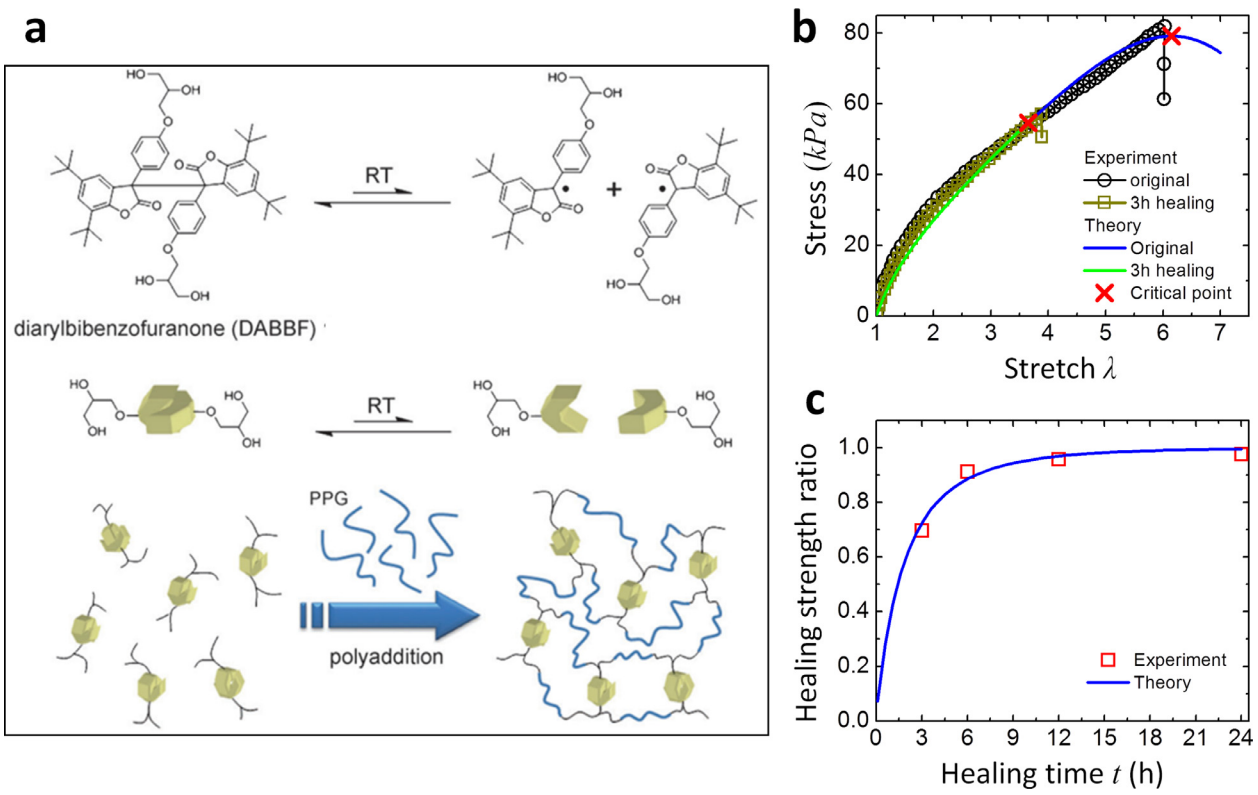

Fig. 11. (a) Chemical structure and reactions of diarylbibenzofuranone (DABBF) (Imato et al., 2012). The experimentally measured and theoretically predicted (b) stress-stretch curves of the original and self-healed samples, and (c) healing strength ratios in a function of the healing time. The graph in (a) and the experimental data in (bc) are reproduced from reference (Imato et al., 2012) with permission. The used parameters can be found in Table 2.

4. Comparison with experimental results

In Section 3, we present general results of the theoretical models of the original and self-healed DPNs. In this section, we will compare the theoretical results with the experimental results. We show our model is very generic and can be applied to understanding a number of DPNs with a variety of dynamic bonds, including dynamic covalent bonds, hydrogen bonds, and ionic bonds.

4.1. DPNs crosslinked by dynamic covalent bonds

We show our model can be used to explain the self-healing polymers with dynamic covalent bonds (Chen et al., 2002; Ghosh and Urban, 2009; Imato et al., 2012; Lu and Guan, 2012; Skene and Lehn, 2004). The first example is a self-healing polymeric gel crosslinked by dynamic covalent bond Diarylbibenzofuranone (DABBF) (Fig. 11a) (Imato et al., 2012). DABBF is a dimer of arylbenzofuranone (ABF) that can be reversibly transformed to two radical species by cleaving the DABBF tolerate oxygen under a sufficiently large chain force. When these two radicals contact back, it can form DABBF again at room temperature. DABBF can crosslink the toluene-2,4-diisocyanate-terminated poly(propylene glycol) (PPG) through a polyaddition reaction with the presence of a catalyst di-n-butyltin dilaurate. This polymeric gel exhibits more than 90% strength healing for 6 h at room temperature. The corresponding experimental results are shown in Fig. 11b and c. Using our model described in Section 2, we can choose adequate model parameters to consistently match the experimentally measured stress-stretch behaviors of the original and self-healed samples (Fig. 11b, parameters in Table 2). In addition, the theoretically calculated healing ratio-time relationship also shows a good agreement with the experimentally measured results (Fig. 11c). It is noted that we only consider the stretching free energy of the polymer network but neglect the solvent-induced missing free energy in Eqs. (8) and (32). It is because the time scale of solvent diffusion within the gel matrix (e.g., 30 min) is usually much larger than the experimental testing time scale (e.g., 3 min); then the mixing free energy of the gel can be assumed as a constant during the mechanical testing process (Wang and Gao, 2016; Wang et al., 2017).

Our model can also be used to explain the self-healing behaviors of DPNs crosslinked by other dynamic covalent bonds, such as reversible C–C double bonds enabled by the olefin metathesis reaction (Lu and Guan, 2012). Olefin metathesis is an organic reaction that enables the redistribution of alkenes (or olefins) by the scission and regeneration of C–C double bonds. Lu and Guan reported a polymer with polybutadiene networks crosslinked by Ru-catalyzed olefin metathesis

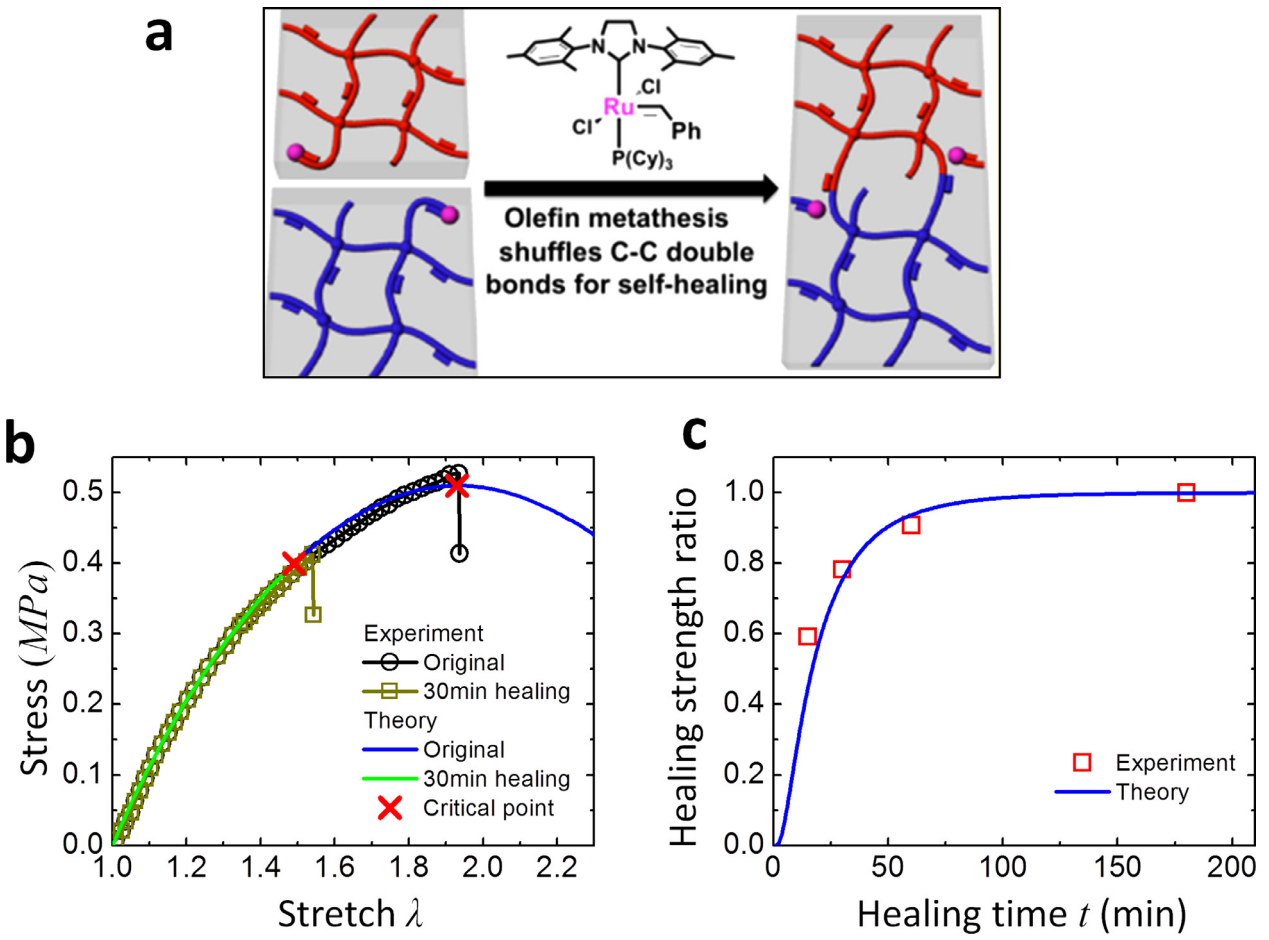

Fig. 12. (a) Olefin metathesis enabled reversible reaction (Lu and Guan, 2012). The experimentally measured and theoretically predicted (b) stress-stretch curves of the original and self-healed samples, and (c) healing strength ratios in a function of the healing time. The graph in (a) and the experimental data in (bc) are reproduced from reference (Lu and Guan, 2012) with permission. The used parameters can be found in Table 2.

Table 2
Model parameters used in this paper. The chain dynamics parameters and Rouse friction coefficients are within the reasonable order compared with limited experimental or simulation results in the references (Chapman et al., 1998; Silberstein et al., 2014; Whitlow and Wool, 1991).

Parameter	Definition	Fig. 4	Fig. 7	Fig. 11	Fig. 12	Fig 13	Fig. 14 strong	Fig. 14 weak
k_i^{f0} (s^{-1})	Forward reaction rate	2×10^{-7}	2×10^{-7}	2×10^{-7}	2×10^{-7}	2×10^{-7}	2×10^{-7}	2×10^{-7}
k_i^{0} (s^{-1})	Reverse reaction rate	2×10^{-5}	4×10^{-4}	4×10^{-4}	4×10^{-4}	4×10^{-5}	4×10^{-5}	8×10^{-6}
Δx (m)	Distance along the energy landscape coordinate	4×10^{-9}	3.8×10^{-9}	3.8×10^{-9}	4×10^{-9}	9.4×10^{-10}	9×10^{-10}	4×10^{-9}
b (m)	Kuhn segment length	5.2×10^{-10}	5.2×10^{-10}	5.2×10^{-10}	5.2×10^{-10}	5.2×10^{-10}	5.2×10^{-10}	
n_1	Minimum chain length	NA	50	50	20	20	700	
n_m	Maximum chain length	NA	1500	1500	200	160	3500	
n_a	Average chain length	NA	690	690	71	64	1600	
δ	Chain length distribution width	NA	0.2	0.2	0.2	0.2	0.2	
α	Chain alteration parameter	NA	0	0	0	0.9	0.05	0.3
ξ (N/m)	Rouse friction coefficient	NA	2.3×10^{-4}	2.3×10^{-4}	2×10^{-3}	1×10^{-2}	1.5×10^{-4}	

(Fig. 12a) (Lu and Guan, 2012). The demonstrated polymers show efficient self-repairing capability, with more than 90% healing within 1 h or shorter depending on the concentration of the Ru catalyst. As shown in Fig. 12b, our model with adequate model parameters can nicely capture the stress-stretch behaviors of the original and self-healed polymer samples (parameters in Table 2). The theoretically calculated healing ratio-time curve can also consistently match the experimentally measured results (Fig. 12c).

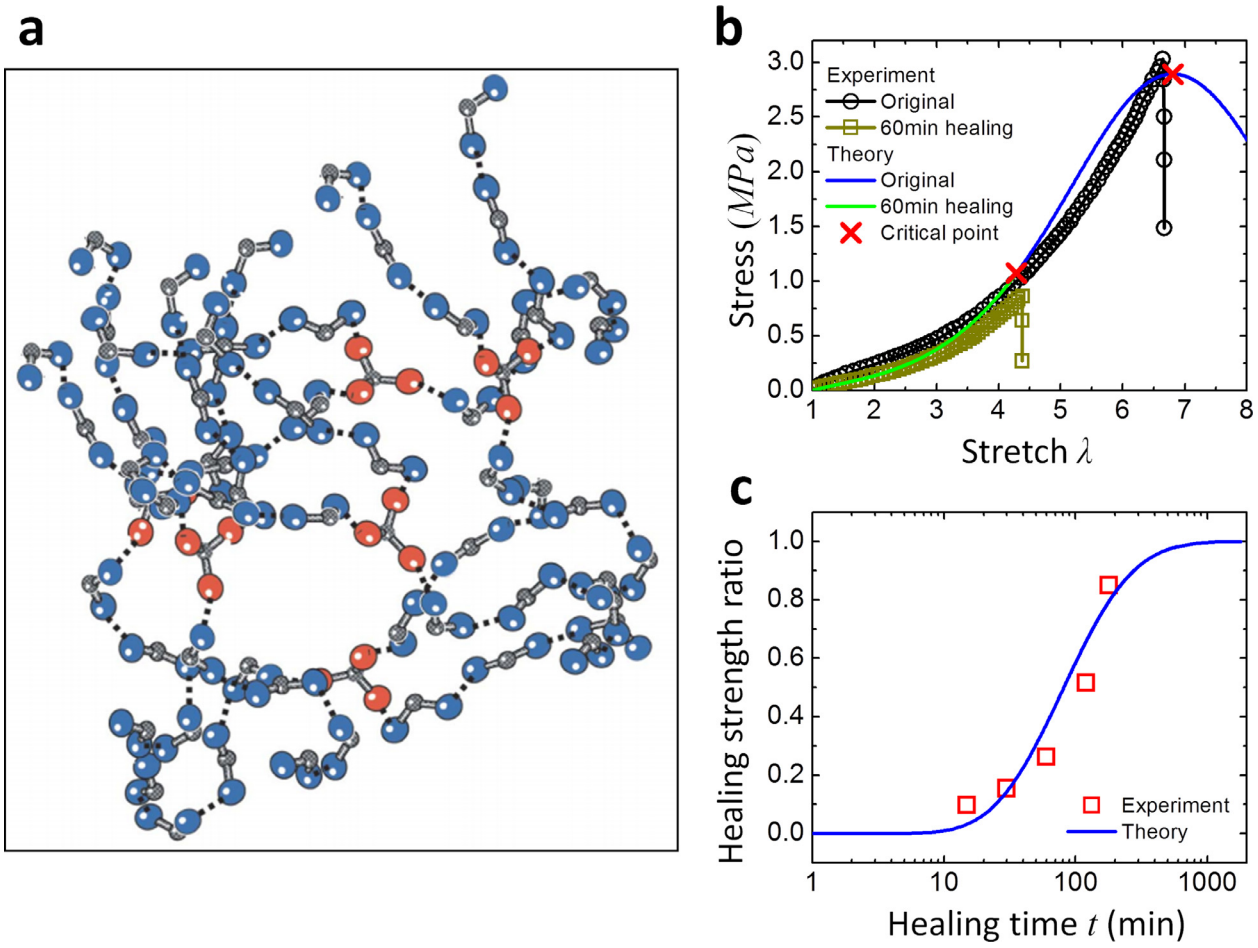

Fig. 13. (a) Schematic of a hydrogen bond crosslinked polymer network (Cordier et al., 2008). The experimentally measured and theoretically predicted (b) stress-stretch curves of the original and self-healed samples, and (c) healing strength ratios in a function of the healing time. The graph in (a) and the experimental data in (bc) are reproduced from reference (Cordier et al., 2008) with permission. The used parameters can be found in Table 2.

4.2. DPNs crosslinked by hydrogen bonds

Hydrogen bonds stem from the electrostatic attraction between hydrogen (H) atom and a highly electronegative atom such as nitrogen (N), oxygen (O), or fluorine (F). These hydrogen bonds can be easily dissociated under external forces, and reform when two groups contact again. Hydrogen bonds have been employed to crosslink polymer networks to enable efficient self-healing capability (Chen et al., 2012; Cordier et al., 2008; Montarnal et al., 2009; Phadke et al., 2012; Sijbesma et al., 1997; Wang et al., 2013a). For example, Cordier et al. (2008) reported a self-healing rubber that harnessed the hydrogen bonds between carboxylic-acid ends and amide groups in amidoethyl imidazolidone, di(amido ethyl) urea, and diamido tetraethyl triurea (Fig. 13a). This rubber exhibited an outstanding stretchability up to more than 500% strain and impressive self-healing capability with nearly 90% strength healing within 3 h. With our theory models, we can theoretically capture the stress-stretch behaviors of the original and self-healed rubber samples under the uniaxial stretch (Fig. 13b). The theoretically calculated healing ratio-time relationship can also roughly match the experimentally measured results (Fig. 13c).

Within the rubber matrix, carboxylic-acid ends can form multiple hydrogen bonds with the amide groups in the polymer chains. When one hydrogen bond is dissociated under stretch, the polymer chain may not become inactive immediately, but form a longer active chain within the matrix (Chagnon et al., 2006; Marckmann et al., 2002). Therefore, in modeling this hydrogen-enabled self-healing DPN, we introduce the effect of the chain alteration described in Section 2.1.3 with the chain alteration parameter$\alpha = 0.9$. The chain alteration effect facilitates to display the stiffening shape of the stress-stretch curve in the large stretch range. More discussions regarding the effect of chain alteration parameters on the stress-stretch behaviors can be found in references (Wang and Gao, 2016; Zhao, 2012).

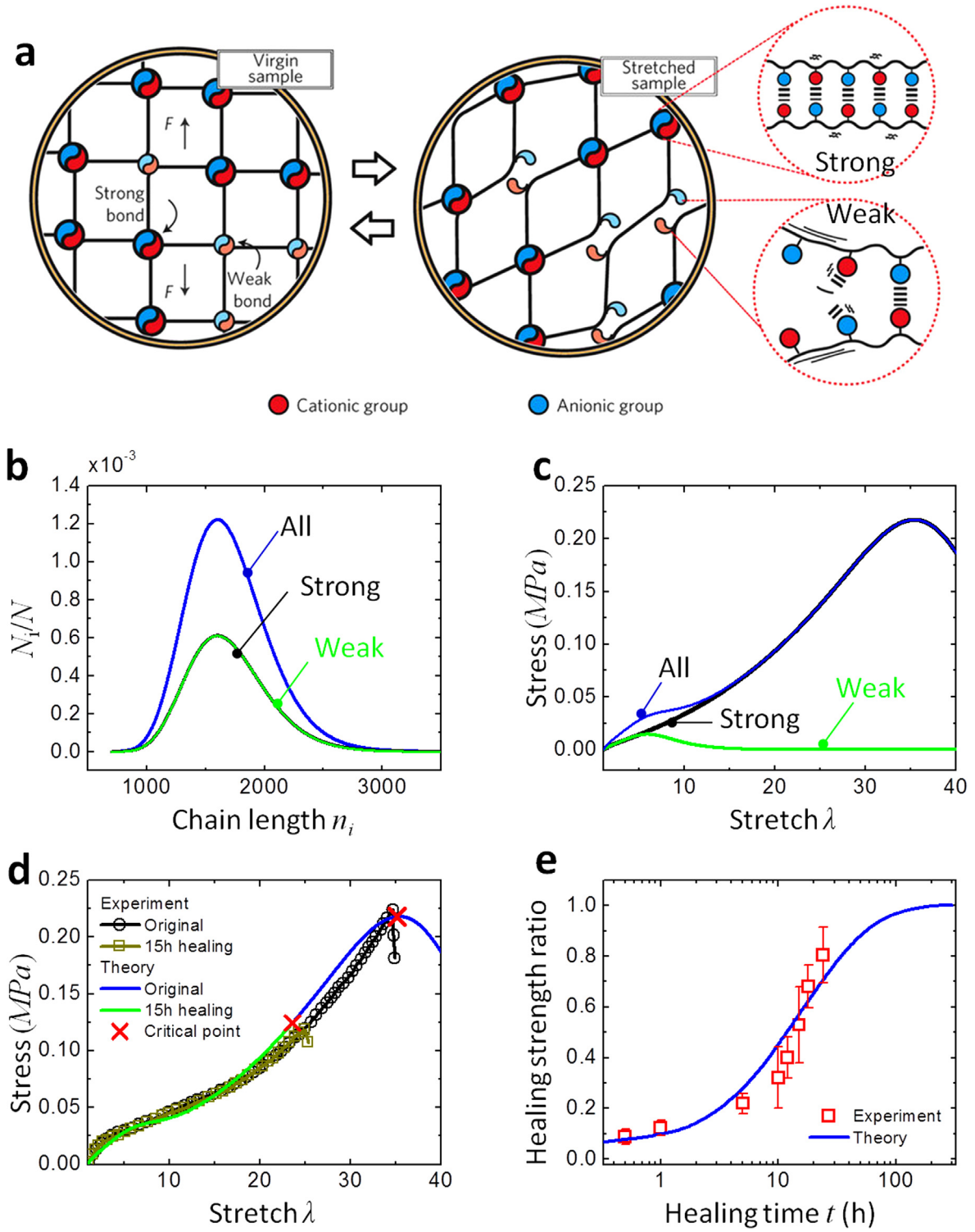

Fig. 14. (a) Schematic of a polymer network crosslinked by strong and weak ionic bonds (Sun et al., 2013). (b) Chain-length distributions of all chains, chains crosslinked by strong ionic bonds, and weak ionic bonds, respectively. (c) Predicted stress-stretch behaviors of the networks with strong ionic bonds, weak ionic bonds, and all bonds. The experimentally measured and theoretically predicted (d) stress-stretch curves of the original and self-healed samples, and (e) healing strength ratios in a function of the healing time. The graph in (a) is reproduced from reference (Sun et al., 2013) with permission. The experimental data in (bc) are reproduced from reference (Ihsan et al., 2016) with permission. The used parameters can be found in Table 2.

4.3. DPNs crosslinked by ionic bonds

An ionic bond is a type of chemical bond that involves the electrostatic attraction between the oppositely charged ions. Compared to covalent bonds, ionic bonds are relatively weak so that they can easily be dissociated under external perturbations, and can also reversibly be associated again when the condition is permitted (Das et al., 2015; Haraguchi et al., 2011; Ihsan et al., 2016; Mayumi et al., 2016; Sun et al., 2012; , 2013; Wang et al., 2010). Ionic bonds have been employed to fabricate soft polymers for a long time (Wei et al., 2014); however, traditional soft polymers crosslinked by a single type of ionic bonds are usually weak and brittle, such as alginate hydrogels (Sun et al., 2012). To enable tough hydrogels, Sun and Suo et al. reported a double-network hydrogel with ionic networks and covalent networks; however, the reported hydrogels cannot fully self-heal their mechanical strength because of the presence of the permanent covalent networks (Sun et al., 2012). Later, Sun and Gong et al. reported a hydrogel with two types of ionic bonds, one stronger and the other weaker (Fig. 14a) (Sun et al., 2013). Because only reversible ionic bonds exist in the hydrogel matrix, the hydrogels exhibit outstanding self-healing capability with over 95% strength healing within 24 h (Ihsan et al., 2016; Sun et al., 2013).

To model this DPN with two types of ionic bonds (Ihsan et al., 2016; Sun et al., 2013), we divide the polymer chains into two portions: chains with strong ionic bonds and chains with weak ionic bonds. Both chains follow the similar chain-length distribution. The total chain number can thus be written as

$$N = N_s + N_w = \sum_{i=1}^{m} \phi N_i + \sum_{i=1}^{m} (1-\phi) N_i \tag{38}$$

where N_s and N_w are chain numbers for the polymer chains crosslinked by strong ionic bonds and weak ionic bonds, respectively; and ϕ is the portion ratio of the chains with strong ionic bonds. We plot an example of chain-length distributions with $\phi = 50\%$ in Fig. 14b. Two portions of chains share the same Rouse friction coefficient, but feature different bond-dynamics parameters and chain alteration parameters (Table 2). The DPN portion with weak ionic bonds can be easily dissociated and become inactive; therefore, the peak point of the stress-stretch curve of the weak DPN sets in at a very small stretch (Fig. 14c). However, the DPN portion with strong ionic bonds remains resilient over a large range of stretch and exhibit a stiffening region at the large-stretch region (Fig. 14c). As a summation, the stress-stretch curve of the total DPN exhibits multiple regions over the whole stretch range (Fig. 14c). In the small stretch region, the whole DPN exhibits a relatively large tangent modulus and then rapidly softens due to the dissociation of the weak DPN; thereafter, the DPN exhibits a stiffening region to primarily display the behavior of the strong DPN until reaching the peak point. Our theoretically calculated stress-stretch behavior of the original DPN can consistently match the experimentally measured results (Fig. 14d). It is particularly noted that only strong DPN portion cannot capture the stress-stretch behaviors at the small stretch region (e.g., stretch = 1–8).

In modeling the self-healing, we consider the strong and weak DPNs follow different healing time scale with different bond dynamic kinetics parameters. Overall, the theoretically predicted stress-strain behaviors of the self-healed hydrogel sample can consistently match the experimentally measured results (Fig. 14d). The theoretically calculated healing ratio-time curve can also roughly match with the experiments (Fig. 14e). The discrepancy probably comes from the complexity of the real polymer networks that cannot be fully modeled by our simplified interpenetrating network model.

5. Conclusive remarks

In summary, we report a theoretical framework that can analytically model the constitutive behaviors and interfacial self-healing behaviors of DPNs crosslinked by a variety of dynamic bonds, including dynamic covalent bonds, hydrogen bonds, and ionic bonds. We consider that the DPN is composed of interpenetrating networks crosslinked by dynamic bonds. The network chains follow inhomogeneous chain-length distributions and the dynamic bonds obey a force-dependent chemical kinetics. During the self-healing process, we consider the polymer chains diffuse across the interface to reform the dynamic bonds, being captured by a diffusion-reaction model. The theories can predict the stress-stretch behaviors of original and self-healed DPNs, as well as the corresponding healing strength over the healing time. We show that the theoretically predicted healing behaviors can consistently match the documented experimental results of DPNs with various dynamic bonds, including dynamic covalent bonds (diarylbibenzofuranone and olefin metathesis), hydrogen bonds, and ionic bonds. We expect that our model can be further extended to explain the self-healing behaviors of DPNs with a wide range of dynamic bonds (Binder, 2013; Roy et al., 2015; Taylor, 2016; Thakur and Kessler, 2015; van der Zwaag, 2007; Wei et al., 2014; Wojtecki et al., 2011; Wu et al., 2008; Yang and Urban, 2013).

Despite the shown salient capability of the current model system, it may also leave a number of open questions. These open questions may forecast a number of future research possibilities. First, the choice of the bond dynamics parameters and Rouse friction coefficient is primarily determined by the exhibited macroscopic experimental results (Table 2 parameters for Figs. 11–14). These parameters are within the reasonable order compared with limited experimental or simulation results in the references (Chapman et al., 1998; Silberstein et al., 2014; Whitlow and Wool, 1991). The requirement of these physical parameters poses an urgent demand for the atomic dynamics simulations or experiments to determine these parameters.

Second, the model system presents an opportunity to model DPNs with very complex network geometries (Creton, 2017; Zhao, 2014, 2017). For example, Wang and Bao et al. reported a metal-ligand coordination crosslinked soft polymer that exhibits ultrahigh stretchability and efficient self-healing (Wang et al., 2013b). The metal-ligand coordination crosslinked

polymer chains are sequentially released and stretched out under the chain force. This self-healing polymer cannot be modeled by the current theory system in this paper; however, involving the consideration of the special sequential-releasing network behaviors may forecast the future possibility.

Third, the current theory system only models the simple geometry of the uniaxial bar stretching. Modeling the self-healing behaviors of more complex geometries to guide the future self-healing practice may demand a sophisticated finite element simulation method; however, such a mature finite-element method to fully model the self-healing mechanics of DPNs is still unavailable (Yu et al., 2016b).

Fourth, the current theory employs the simplest interpenetration network model with an assumption that polymer chains within a network feature the same chain length and different networks interpenetrate into each other (Wang et al., 2015). The assumption would lead to a subsequent assumption that the association-dissociation bond dynamics only occur among chains with the same chain length. These restrictions can be relaxed by considering the connection of chains with dissimilar chain lengths (Verron and Gros, 2017). If so, the same chain force will induce imbalance stretches to different chains within a network, and diffusion time-scales for these different chains are also different. A more sophisticated statistical averaging model should be considered to address these issues.

Acknowledgement

Q.W. acknowledges the funding support from Air Force Office of Scientific Research Young Investigator Program and National Science Foundation (CMMI-1649093, CMMI-1762567).

Supplementary materials

Supplementary material associated with this article can be found, in the online version, at doi:10.1016/j.jmps.2018.08.007.

References

Arruda, E.M., Boyce, M.C., 1993. A three-dimensional constitutive model for the large stretch behavior of rubber elastic materials. J. Mech. Phys. Solids. 41, 389–412.
Balazs, A.C., 2007. Modeling self-healing materials. Mater. Today 10, 18–23.
Bell, G.I., 1978. Models for the specific adhesion of cells to cells. Science 200, 618–627.
Binder, W.H., 2013. Self-healing polymers: from principles to applications. John Wiley & Sons.
Blaiszik, B., Kramer, S., Olugebefola, S., Moore, J.S., Sottos, N.R., White, S.R., 2010. Self-healing polymers and composites. Annu. Rev. Mater. Res. 40, 179–211.
Brochu, A.B., Craig, S.L., Reichert, W.M., 2011. Self-healing biomaterials. J.Biomed. Mater. Res. Part A 96, 492–506.
Burnworth, M., Tang, L., Kumpfer, J.R., Duncan, A.J., Beyer, F.L., Fiore, G.L., Rowan, S.J., Weder, C., 2011. Optically healable supramolecular polymers. Nature 472, 334–337.
Carlsson, L., Rose, S., Hourdet, D., Marcellan, A., 2010. Nano-hybrid self-crosslinked PDMA/silica hydrogels. Soft Matter 6, 3619–3631.
Chagnon, G., Verron, E., Marckmann, G., Gornet, L., 2006. Development of new constitutive equations for the Mullins effect in rubber using the network alteration theory. Int. J. Solids. Struct. 43, 6817–6831.
Chapman, B.R., Hamersky, M.W., Milhaupt, J.M., Kostelecky, C., Lodge, T.P., von Meerwall, E.D., Smith, S.D., 1998. Structure and dynamics of disordered tetrablock copolymers: composition and temperature dependence of local friction. Macromolecules 31, 4562–4573.
Chen, X., Dam, M.A., Ono, K., Mal, A., Shen, H., Nutt, S.R., Sheran, K., Wudl, F., 2002. A thermally re-mendable cross-linked polymeric material. Science 295, 1698–1702.
Chen, Y., Kushner, A.M., Williams, G.A., Guan, Z., 2012. Multiphase design of autonomic self-healing thermoplastic elastomers. Nat. Chem 4, 467–472.
Cho, S.H., Andersson, H.M., White, S.R., Sottos, N.R., Braun, P.V., 2006. Polydimethylsiloxane-based self-healing materials. Adv. Mater. 18, 997–1000.
Cordier, P., Tournilhac, F., Soulié-Ziakovic, C., Leibler, L., 2008. Self-healing and thermoreversible rubber from supramolecular assembly. Nature 451, 977–980.
Crank, J., 1979. The Mathematics of Diffusion. Oxford University Press.
Creton, C., 2017. 50th anniversary perspective: networks and gels: soft but dynamic and tough. Macromolecules 50, 8297–8316.
Das, A., Sallat, A., Böhme, F., Suckow, M., Basu, D., Wießner, S., Stöckelhuber, K.W., Voit, B., Heinrich, G., 2015. Ionic modification turns commercial rubber into a self-healing material. ACS Appl. Mater. Interfaces 7, 20623–20630.
Davidson, J.D., Goulbourne, N., 2013. A nonaffine network model for elastomers undergoing finite deformations. J. Mech. Phys. Solids. 61, 1784–1797.
Doi, M., Edwards, S.F., 1978. Dynamics of concentrated polymer systems. Part 1.-Brownian motion in the equilibrium state. J. Chem. Soc. Faraday Trans 74, 1789–1801.
Doi, M., Edwards, S.F., 1988. The Theory of Polymer Dynamics. Oxford University Press.
Erman, B., Mark, J.E., 1997. Structures and Properties of Rubberlike Networks. Oxford University Press, Oxford.
Fox, J., Wie, J.J., Greenland, B.W., Burattini, S., Hayes, W., Colquhoun, H.M., Mackay, M.E., Rowan, S.J., 2012. High-strength, healable, supramolecular polymer nanocomposites. J. Am. Chem. Soc. 134, 5362–5368.
de Gennes, P.-G., 1979. Scaling Concepts in Polymer Physics.
de Gennes, P.G., 1971. Reptation of a polymer chain in the presence of fixed obstacles. J. Chem. Phys. 55, 572–579.
Ge, T., Robbins, M.O., Perahia, D., Grest, G.S., 2014. Healing of polymer interfaces: Interfacial dynamics, entanglements, and strength. Phys. Rev. E 90, 012602.
Ghosh, B., Urban, M.W., 2009. Self-repairing oxetane-substituted chitosan polyurethane networks. Science 323, 1458–1460.
Gulyuz, U., Okay, O., 2014. Self-healing poly (acrylic acid) hydrogels with shape memory behavior of high mechanical strength. Macromolecules 47, 6889–6899.
Hänggi, P., Talkner, P., Borkovec, M., 1990. Reaction-rate theory: fifty years after Kramers. Rev. Mod. Phys. 62, 251.
Haraguchi, K., 2007. Nanocomposite hydrogels. Curr. Opin. Solid State Mater. Sci. 11, 47–54.
Haraguchi, K., 2011a. Stimuli-responsive nanocomposite gels. Colloid. Polym. Sci. 289, 455–473.
Haraguchi, K., 2011b. Synthesis and properties of soft nanocomposite materials with novel organic/inorganic network structures. Polym. J. 43, 223–241.
Haraguchi, K., Farnworth, R., Ohbayashi, A., Takehisa, T., 2003. Compositional effects on mechanical properties of nanocomposite hydrogels composed of poly (N, N-dimethylacrylamide) and clay. Macromolecules 36, 5732–5741.
Haraguchi, K., Li, H.-J., 2006. Mechanical properties and structure of polymer-clay nanocomposite gels with high clay content. Macromolecules 39, 1898–1905.
Haraguchi, K., Li, H.-J., Song, L., Murata, K., 2007. Tunable optical and swelling/deswelling properties associated with control of the coil-to-globule transition of poly (N-isopropylacrylamide) in polymer-clay nanocomposite gels. Macromolecules 40, 6973–6980.

Haraguchi, K., Li, H.J., 2005. Control of the coil-to-globule transition and ultrahigh mechanical properties of PNIPA in nanocomposite hydrogels. Angew. Chem. Int. Ed. 44, 6500–6504.
Haraguchi, K., Song, L., 2007. Microstructures formed in co-cross-linked networks and their relationships to the optical and mechanical properties of PNIPA/clay nanocomposite gels. Macromolecules 40, 5526–5536.
Haraguchi, K., Takehisa, T., 2002. Nanocomposite hydrogels: a unique organic-inorganic network structure with extraordinary mechanical, optical, and swelling/de-swelling properties. Adv. Mater. 14, 1120–1124.
Haraguchi, K., Takehisa, T., Fan, S., 2002. Effects of clay content on the properties of nanocomposite hydrogels composed of poly (N-isopropylacrylamide) and clay. Macromolecules 35, 10162–10171.
Haraguchi, K., Uyama, K., Tanimoto, H., 2011. Self-healing in nanocomposite hydrogels. Macromol. Rapid Commun. 32, 1253–1258.
Holten-Andersen, N., Harrington, M.J., Birkedal, H., Lee, B.P., Messersmith, P.B., Lee, K.Y.C., Waite, J.H., 2011. pH-induced metal-ligand cross-links inspired by mussel yield self-healing polymer networks with near-covalent elastic moduli. Proc. Natl. Acad. Sci. USA 108, 2651–2655.
Huang, T., Xu, H., Jiao, K., Zhu, L., Brown, H.R., Wang, H., 2007. A novel hydrogel with high mechanical strength: a macromolecular microsphere composite hydrogel. Adv. Mater. 19, 1622–1626.
Hui, C.-Y., Long, R., 2012. A constitutive model for the large deformation of a self-healing gel. Soft Matter 8, 8209–8216.
Ihsan, A.B., Sun, T.L., Kurokawa, T., Karobi, S.N., Nakajima, T., Nonoyama, T., Roy, C.K., Luo, F., Gong, J.P., 2016. Self-healing behaviors of tough polyampholyte hydrogels. Macromolecules 49, 4245–4252.
Imato, K., Nishihara, M., Kanehara, T., Amamoto, Y., Takahara, A., Otsuka, H., 2012. Self-healing of chemical gels cross-linked by diarylbibenzofuranone-based trigger-free dynamic covalent bonds at room temperature. Angew. Chem. Int. Ed. 51, 1138–1142.
Iyer, B.V., Yashin, V.V., Kowalewski, T., Matyjaszewski, K., Balazs, A.C., 2013. Strain recovery and self-healing in dual cross-linked nanoparticle networks. Polym. Chem. 4, 4927–4939.
Keller, M.W., White, S.R., Sottos, N.R., 2007. A self-healing poly (dimethyl siloxane) elastomer. Adv. Funct. Mater. 17, 2399–2404.
Kersey, F.R., Loveless, D.M., Craig, S.L., 2007. A hybrid polymer gel with controlled rates of cross-link rupture and self-repair. J. R. Soc. Interface 4, 373–380.
Khiêm, V.N., Itskov, M., 2016. Analytical network-averaging of the tube model: rubber elasticity. J. Mech. Phys. Solids. 95, 254–269.
Kim, Y.H., Wool, R.P., 1983. A theory of healing at a polymer-polymer interface. Macromolecules 16, 1115–1120.
Kramers, H.A., 1940. Brownian motion in a field of force and the diffusion model of chemical reactions. Physica 7, 284–304.
Lake, G., Thomas, A., 1967. The strength of highly elastic materials. Proc. R. Soc. Lond. A 300, 108–119.
Li, Y., Tang, S., Kröger, M., Liu, W.K., 2016. Molecular simulation guided constitutive modeling on finite strain viscoelasticity of elastomers. J. Mech. Phys. Solids. 88, 204–226.
Liu, J., Tan, C.S.Y., Yu, Z., Lan, Y., Abell, C., Scherman, O.A., 2017a. Biomimetic supramolecular polymer networks exhibiting both toughness and self-recovery. Adv. Mater 29, 1604951.
Liu, J., Tan, C.S.Y., Yu, Z., Li, N., Abell, C., Scherman, O.A., 2017b. Tough supramolecular polymer networks with extreme stretchability and fast room-temperature self-healing. Adv. Mater. 29, 1605325.
Long, R., Mayumi, K., Creton, C., Narita, T., Hui, C.-Y., 2014. Time dependent behavior of a dual cross-link self-healing gel: theory and experiments. Macromolecules 47, 7243–7250.
Lu, Y.-X., Guan, Z., 2012. Olefin metathesis for effective polymer healing via dynamic exchange of strong carbon–carbon double bonds. J. Am. Chem. Soc. 134, 14226–14231.
Marckmann, G., Verron, E., Gornet, L., Chagnon, G., Charrier, P., Fort, P., 2002. A theory of network alteration for the Mullins effect. J. Mech. Phys. Solids. 50, 2011–2028.
Mayumi, K., Guo, J., Narita, T., Hui, C.Y., Creton, C., 2016. Fracture of dual crosslink gels with permanent and transient crosslinks. Extreme Mech. Lett. 6, 52–59.
Montarnal, D., Tournilhac, F., Hidalgo, M., Couturier, J.-L., Leibler, L., 2009. Versatile one-pot synthesis of supramolecular plastics and self-healing rubbers. J. Am. Chem. Soc. 131, 7966–7967.
Nakahata, M., Takashima, Y., Yamaguchi, H., Harada, A., 2011. Redox-responsive self-healing materials formed from host–guest polymers. Nat. Comm. 2, 511.
Okay, O., 2015. Self-Healing Hydrogels Formed Via Hydrophobic Interactions, Supramolecular Polymer Networks and Gels. Springer, pp. 101–142.
Phadke, A., Zhang, C., Arman, B., Hsu, C.-C., Mashelkar, R.A., Lele, A.K., Tauber, M.J., Arya, G., Varghese, S., 2012. Rapid self-healing hydrogels. Proc. Natl. Acad. Sci. USA 109, 4383–4388.
Ren, H.-Y., Zhu, M., Haraguchi, K., 2011. Characteristic swelling–deswelling of polymer/clay nanocomposite gels. Macromolecules 44, 8516–8526.
Ribas-Arino, J., Marx, D., 2012. Covalent mechanochemistry: theoretical concepts and computational tools with applications to molecular nanomechanics. Chem. Rev. 112, 5412–5487.
Rowan, S.J., Beck, J.B., 2005. Metal–ligand induced supramolecular polymerization: a route to responsive materials. Faraday Discuss. 128, 43–53.
Roy, N., Bruchmann, B., Lehn, J.-M., 2015. DYNAMERS: dynamic polymers as self-healing materials. Chem. Soc. Rev. 44, 3786–3807.
Rubinstein, M., Colby, R., 2003. Polymer Physics. Oxford University Press, Oxford.
Sijbesma, R.P., Beijer, F.H., Brunsveld, L., Folmer, B.J., Hirschberg, J.K., Lange, R.F., Lowe, J.K., Meijer, E., 1997. Reversible polymers formed from self-complementary monomers using quadruple hydrogen bonding. Science 278, 1601–1604.
Silberstein, M.N., Cremar, L.D., Beiermann, B.A., Kramer, S.B., Martinez, T.J., White, S.R., Sottos, N.R., 2014. Modeling mechanophore activation within a viscous rubbery network. J. Mech. Phys. Solids. 63, 141–153.
Skene, W.G., Lehn, J.-M.P., 2004. Dynamers: polyacylhydrazone reversible covalent polymers, component exchange, and constitutional diversity. Proc. Natl. Acad. Sci. USA 101, 8270–8275.
Stukalin, E.B., Cai, L.-H., Kumar, N.A., Leibler, L., Rubinstein, M., 2013. Self-healing of unentangled polymer networks with reversible bonds. Macromolecules 46, 7525–7541.
Sun, J.-Y., Zhao, X., Illeperuma, W.R., Chaudhuri, O., Oh, K.H., Mooney, D.J., Vlassak, J.J., Suo, Z., 2012. Highly stretchable and tough hydrogels. Nature 489, 133–136.
Sun, T.L., Kurokawa, T., Kuroda, S., Ihsan, A.B., Akasaki, T., Sato, K., Haque, M.A., Nakajima, T., Gong, J.P., 2013. Physical hydrogels composed of polyampholytes demonstrate high toughness and viscoelasticity. Nat. Mater. 12, 932–937.
Taylor, D.L., 2016. Self-healing hydrogels. Adv. Mater. 28, 9060–9093.
Tee, B.C., Wang, C., Allen, R., Bao, Z., 2012. An electrically and mechanically self-healing composite with pressure-and flexion-sensitive properties for electronic skin applications. Nat. Nanotechnol. 7, 825–832.
Terryn, S., Brancart, J., Lefeber, D., Van Assche, G., Vanderborght, B., 2017. Self-healing soft pneumatic robots. Sci. Robot. 2 eaan4268.
Thakur, V.K., Kessler, M.R., 2015. Self-healing polymer nanocomposite materials: a review. Polymer 69, 369–383.
Toohey, K.S., Sottos, N.R., Lewis, J.A., Moore, J.S., White, S.R., 2007. Self-healing materials with microvascular networks. Nat. Mater. 6, 581–585.
Treloar, L.R.G., 1975. The Physics of Rubber Elasticity. Oxford University Press, Oxford.
Verron, E., Gros, A., 2017. An equal force theory for network models of soft materials with arbitrary molecular weight distribution. J. Mech. Phys. Solids. 106, 176–190.
Wang, C., Liu, N., Allen, R., Tok, J.B.H., Wu, Y., Zhang, F., Chen, Y., Bao, Z., 2013a. A rapid and efficient self-healing thermo-reversible elastomer crosslinked with graphene oxide. Adv. Mater. 25, 5785–5790.
Wang, C., Wu, H., Chen, Z., McDowell, M.T., Cui, Y., Bao, Z., 2013b. Self-healing chemistry enables the stable operation of silicon microparticle anodes for high-energy lithium-ion batteries. Nat. Chem. 5, 1042–1048.
Wang, Q., Gao, Z., 2016. A constitutive model of nanocomposite hydrogels with nanoparticle crosslinkers. J. Mech. Phys. Solids. 94, 127–147.
Wang, Q., Gao, Z., Yu, K., 2017. Interfacial self-healing of nanocomposite hydrogels: theory and experiment. J. Mech. Phys. Solids. 109, 288–306.

Wang, Q., Gossweiler, G.R., Craig, S.L., Zhao, X., 2015. Mechanics of mechanochemically responsive elastomers. J. Mech. Phys. Solids 82, 320–344.
Wang, Q., Mynar, J.L., Yoshida, M., Lee, E., Lee, M., Okuro, K., Kinbara, K., Aida, T., 2010. High-water-content mouldable hydrogels by mixing clay and a dendritic molecular binder. Nature 463, 339–343.
Wei, Z., Yang, J.H., Zhou, J., Xu, F., Zrínyi, M., Dussault, P.H., Osada, Y., Chen, Y.M., 2014. Self-healing gels based on constitutional dynamic chemistry and their potential applications. Chem. Soc. Rev. 43, 8114–8131.
White, S.R., Sottos, N., Geubelle, P., Moore, J., Kessler, M.R., Sriram, S., Brown, E., Viswanathan, S., 2001. Autonomic healing of polymer composites. Nature 409, 794–797.
Whitlow, S.J., Wool, R.P., 1991. Diffusion of polymers at interfaces: a secondary ion mass spectroscopy study. Macromolecules 24, 5926–5938.
Wojtecki, R.J., Meador, M.A., Rowan, S.J., 2011. Using the dynamic bond to access macroscopically responsive structurally dynamic polymers. Nat. Mater. 10, 14–27.
Wool, R., O'connor, K., 1981. A theory crack healing in polymers. J. Appl. Phys. 52, 5953–5963.
Wool, R.P., 1995. Polymer interfaces: structure and strength. Hanser.
Wool, R.P., 2008. Self-healing materials: a review. Soft Matter 4, 400–418.
Wu, D.Y., Meure, S., Solomon, D., 2008. Self-healing polymeric materials: a review of recent developments. Prog. Polym. Sci. 33, 479–522.
Xiang, Y., Zhong, D., Wang, P., Mao, G., Yu, H., Qu, S., 2018. A general constitutive model of soft elastomers. J. Mech. Phys. Solids. 117, 110–122.
Yang, Y., Urban, M.W., 2013. Self-healing polymeric materials. Chem. Soc. Rev 42, 7446–7467.
Yu, K., Shi, Q., Li, H., Jabour, J., Yang, H., Dunn, M.L., Wang, T., Qi, H.J., 2016a. Interfacial welding of dynamic covalent network polymers. J. Mech. Phys. Solids. 94, 1–17.
Yu, K., Shi, Q., Wang, T., Dunn, M.L., Qi, H.J., 2016b. A computational model for surface welding in covalent adaptable networks using finite element analysis. J.Appl. Mech. 83, 091002.
Zhang, H., Wool, R.P., 1989. Concentration profile for a polymer-polymer interface. 1. Identical chemical composition and molecular weight. Macromolecules 22, 3018–3021.
Zhang, M.Q., Rong, M.Z., 2012. Theoretical consideration and modeling of self-healing polymers. J. Polym. Sci. Part B: Polym. Phys. 50, 229–241.
Zhao, X., 2012. A theory for large deformation and damage of interpenetrating polymer networks. J. Mech. Phys. Solids. 60, 319–332.
Zhao, X., 2014. Multi-scale multi-mechanism design of tough hydrogels: building dissipation into stretchy networks. Soft Matter 10, 672–687.
van der Zwaag, S., 2007. Self Healing Materials: An Alternative Approach to 20 Centuries of Materials Science. Springer Science & Business Media.
Zhao, X., 2017. Designing toughness and strength for soft materials. Proc. Natl. Acad. Sci. 114, 8138–8140.